https://doi.org/10.5194/egusphere-2026-2896
Preprint. Discussion started: 6 July 2026

Observations of radiocarbon (^{14}C) in atmospheric CO_2 confirm decline in U.S. emissions of fossil fuel CO_2 ($FFCO_2$) between 2010 and 2015

S M Nazrul Islam[1,2,8,9], Scott J. Lehman[3], Sourish Basu[4,5], Arlyn E. Andrews[2,7], Kathryn McKain[2], Colm Sweeney[2], Xiaomei Xu[6], Chad Wolak[3], Stephen P. Morgan[3], Patrick Cappa[3], John R. Southon[6], Pieter P. Tans[3], John B. Miller[2]

[1]Cooperative Institute for Research in Environmental Sciences, University of Colorado Boulder, Boulder, CO 80309
[2]NOAA Global Monitoring Laboratory, Boulder, CO 80305
[3]Institute of Arctic and Alpine Research, University of Colorado Boulder, Boulder, CO 80309
[4]Global Modeling and Assimilation Office, NASA Goddard Space Flight Center, Greenbelt, MD 20771
[5]Earth System Science Interdisciplinary Center, University of Maryland, College Park, MD 20740
[6]Keck Carbon Cycle AMS Facility, University of California, Irvine, CA 92697
[7]now at: SilverLining, Washington, DC 20001
[8]now at: Cooperative Institute for Research in Environmental Sciences, University of Colorado Boulder, Boulder, CO 80309
[9]now at: NOAA Chemical Sciences Laboratory, Boulder, CO 80305

Correspondence to: S M Nazrul Islam (SMNazrul.Islam@colorado.edu; smnazrul818@gmail.com)

Abstract. All emissions pathways aimed at stabilizing global temperatures at the internationally agreed target of 1.5-2 °C above pre-industrial levels require steep cuts in global CO_2 emissions. Reliable emissions tracking is therefore essential to monitoring progress towards related mitigation goals, especially for the world's largest emitters. Here we make use of atmospheric measurements of $\Delta^{14}CO_2$ and the dual-tracer $\Delta^{14}CO_2$:CO_2 assimilation and inversion system previously developed by our group to estimate annual and monthly CO_2 emissions from fossil fuel use and cement production ($FFCO_2$) for the U.S. for 2010 and 2015, the first two individual years for which large numbers of atmospheric $\Delta^{14}CO_2$ measurements are available. Ensemble-mean national $FFCO_2$ totals obtained from a 9-member suite of inverse results are larger than reported by the U.S. Environmental Protection Agency (EPA), but overlap at their respective 2σ ensemble-wide model spreads (inversions) and reported 95% confidence intervals (EPA) in both years. In contrast, the inverse results agree with both annual totals and 16 of 24 derived monthly totals from the Vulcan 3.0 emissions data product with 1σ, ensemble wide. Central estimates of the change in U.S. $FFCO_2$ emission between 2010 and 2015 range from -5.1% (EPA), -5.8% (Vulcan), and -7.8% (this work), providing a first confirmation of an expected national $FFCO_2$ decline based on atmospheric observations. The development of a reliable emissions tracking system based directly on atmospheric observations, as detailed here, may take on additional scientific and policy relevance given the recent interruption of EPA reporting.

https://doi.org/10.5194/egusphere-2026-2896
Preprint. Discussion started: 6 July 2026

1 Introduction

The ongoing climate crisis is in large part a problem of cumulative anthropogenic CO_2 emissions. This is because CO_2 (unlike, for example, methane) is chemically stable in the atmosphere, such that atmospheric CO_2 growth rates are controlled exclusively by the ongoing imbalance between emissions and any net transfers into land and ocean reservoirs. Thus, emissions of CO_2 must fall to levels exceeded by rates of combined net land and ocean removals before atmospheric CO_2 concentrations and the associated radiative climate forcing can begin to decline. Indeed, all emissions pathways consistent with the internationally-agreed target of limiting post-industrial warming to +1.5-2 °C (with or without transient overshoot) call for net CO_2 additions below zero by mid-century, requiring steep cuts in emissions from fossil fuel use and cement production over the next few decades (IPCC, 2018). The international effort under the Paris Agreement to reach this target includes individual Nationally Determined Contributions and country self-reporting on emissions of CO_2 and other greenhouse gases as a means of tracking the efficacy of mitigation measures (UNFCCC, 2015). For the U.S., reporting has been provided by the EPA since the establishment of the United Nations Framework Convention on Climate Change (UNFCCC) in 1992 and has remained the U.S. report of record to the international community (although such reporting was recently halted). While EPA accounting of U.S. CO_2 emissions was designed to be comprehensive, and has included retrospective revisions when warranted, it is a matter of both scientific and policy prudence to expose EPA and other international reporting efforts to independent evaluation. In previous work (Basu et al., 2020), we showed that precise measurements of the radiocarbon (^{14}C) to total C ratio of CO_2 (expressed as $\Delta^{14}C$ or $\Delta^{14}CO_2$) could be used to constrain emissions of CO_2 from fossil fuel combustion and cement production ("fossil CO_2") over the U.S. The method is largely unbiased because, over large, industrialized land areas such as the conterminous U.S., measured gradients of atmospheric $\Delta^{14}CO_2$ are controlled almost exclusively by emission of ^{14}C-free CO_2 from fossil sources (Lehman et al., 2013; Miller et al., 2025b; Miller et al., 2025a; Graven et al., 2012; Miller et al., 2012; Levin et al., 2003). Thus, observations of atmospheric $\Delta^{14}CO_2$ can be traced back to emissions at the surface using inverse methods, providing quantitative constraints on emissions intensity in space and time (Basu et al., 2020; Basu et al., 2016; Potier et al., 2022; Wang et al., 2017). Given adequate measurement coverage with respect to the distribution of emissions and their subsequent dispersion by atmospheric mixing, atmospheric observations inherently sense all emissions and provide a valuable complement to "bottom-up" methods of accounting (so-called "emissions inventories") which rely on comprehensive knowledge of all emissions processes and their intensities. In previous work (Basu et al., 2020), we demonstrated that ^{14}C-based estimates of U.S. fossil CO_2 ($FFCO_2$) emissions for the year 2010 agreed with EPA to within 5%, but were considerably (7-10%) larger than U.S. totals from $FFCO_2$ inventories often used in global CO_2 accounting and inverse modeling studies [i.e., EDGAR (Crippa, 2024), ODIAC (Oda et al., 2018), and FFDAS (Asefi-Najafabady et al., 2014)]. Notably, the ^{14}C-based estimates agreed within their estimated analytical uncertainties of ~2% (1σ) with the 2010 annual total from the U.S. specific Vulcan emissions data product (Gurney et al., 2020b; Gurney et al., 2020a), which ingests additional information not considered explicitly by the EPA (e.g., Kato et al. (2023)).

https://doi.org/10.5194/egusphere-2026-2896
Preprint. Discussion started: 6 July 2026

The importance of tracking $FFCO_2$ emissions as a means of verifying progress towards mitigation targets and informing current and future carbon markets has led to a number of new emissions tracking efforts having high temporal resolution and near global scope. Carbon Monitor (https://carbonmonitor.org), for example, can deliver emissions estimates to policy makers and other stake holders in near-real time, but is reliant on a mix of largely indirect measures of emission intensity (Liu et al., 2020; Liu et al., 2024). Climate Trace (https://climatetrace.org) ingests a wide range of data streams including remotely sensed estimates of emission that may help fill gaps in existing inventories and target the largest polluters (Voosen, 2023). While these approaches aim to be as comprehensive as possible, the ability to capture all emissions at all times is hardly guaranteed and methodological biases and uncertainties are intrinsically difficult to quantify.

Here we present new ^{14}C-based estimates of annual and monthly U.S. $FFCO_2$ emissions for the years 2010 and 2015, using observations drawn primarily from the North American portion of NOAA's Global Greenhouse Gas Reference Network (GGGRN https://gml.noaa.gov/ccgg/about.html), (Andrews et al., 2014; Sweeney et al., 2015) and supplemented by other ^{14}C measurement groups (Table S1). Our initial focus on 2010 and 2015 reflects increased measurement coverage within the GGGRN in those years (NOAA's atmospheric measurement activities were restricted between 2011 and 2014 due to budgetary constraints). In order to objectively compare U.S. $FFCO_2$ emission estimates for 2010 and 2015, we revisited the earlier estimates for 2010 of Basu et al. (2020), assimilating additional CO_2 measurements from a retrospective update of global and North American CO_2 observations compiled in NOAA's ObsPack GLOBALVIEWplus collection 6.1 ("GV+6.1") data product (Schuldt et al., 2021) and other improvements to the data assimilation system discussed below. The new results confirm reductions of U.S. $FFCO_2$ between 2010 and 2015 based on reports for those years by the EPA (EPA, 2024a) and from the Vulcan data product (Gurney et al., 2020b; Gurney et al., 2020a) , and represent a first step towards providing a more complete analysis of the inter-annual variability and trends in U.S. emissions across the full decade of the 2010s. Once established, ongoing assimilation of $^{14}CO_2$ and CO_2 observations from within the GGGRN and collaborating measurement programs can provide regular yearly estimates of U.S. national and regional fossil CO_2 emissions. Ongoing agreement between $FFCO_2$ flux estimates of the EPA, the Vulcan emissions data product, and from assimilation of atmospheric $\Delta^{14}CO_2$ measurements would suggest a highly complementary national $FFCO_2$ observing system, in which the top-down approach provides national- to regional-scale integral constraints on total emissions while ^{14}C-verified "bottom-up" products continue to provide important information on emissions from different economic sectors which can together inform policy with a high degree of scientific confidence.

2 Methods and Experimental Design

2.1 Inverse modelling system

We use the dual-tracer variational inversion framework (TM5 4DVar) of our previous studies (Basu et al., 2016; Basu et al., 2020), which minimizes the cost function

https://doi.org/10.5194/egusphere-2026-2896
Preprint. Discussion started: 6 July 2026

$$J = \left(y - H(x)\right)^T R^{-1}\left(y - H(x)\right) + \left(x - x_p\right)^T B^{-1}\left(x - x_p\right) \quad \text{(eq. 1)}$$

in order to optimize the estimation of fossil, Net Biome Exchange (NBE = NEE or Net Ecosystem Exchange + fire), net ocean, and ^{14}C-specific fluxes (in vector $\boldsymbol{x}$) by simultaneously assimilating globally distributed measurements of atmospheric CO_2 and $\Delta^{14}C$ (contained in vector y). The TM5 global transport model (represented in eq. 1 by the operator H) is driven by the most recent ECMWF reanalysis, ERA5 (Hersbach et al., 2020), and is run at a resolution of 3° (longitude) × 2° (latitude) globally and 1° x 1° over North America (20-64° N, 132-60° W), where ERA5 is a relatively minor update to the ERA-Interim reanalysis (Dee et al., 2011; Hoffmann et al., 2019) used as meteorological forcing in our previous work (Basu et al., 2020; Basu et al., 2016). As shown in the previous studies, TM5 accurately simulates pole-to-pole meridional and North American vertical gradients of SF_6 (an inert tracer with a relatively well-known source distribution similar to that of $FFCO_2$), suggesting that characteristics of the large-scale transport are well represented by the model. Details regarding error covariance matrices for model-data-mismatch (R) and prior fluxes (B) (eq. 1), as well as other technical aspects of the inversions are provided in the Supplemental Information (SI).

For 2010, we implemented initial three-dimensional fields for both $\Delta^{14}CO_2$ and CO_2 developed earlier in Basu et al. (2020). For 2015, initial fields were obtained from the end of the first inversion period and scaled by the time dependent change in background $\Delta^{14}C$ observations from the end of the 2010 inversion period to the beginning of the 2015 inversion period. For both 2010 and 2015, inversions started July 1 (either 2009 or 2014) and ended April 1 (either 2011 or 2016). System sensitivity to alternative durations and methods of initialization is discussed in the SI.

2.2 Observations

The current system assimilates CO_2 observations from NOAA's ObsPack GV+6.1 (Schuldt et al., 2021) and $\Delta^{14}CO_2$ observations coming largely from the North American portion of the NOAA Global Greenhouse Gas Reference Network (GGGRN, https://gml.noaa.gov/ccgg/about.html) (Andrews et al., 2014; Sweeney et al., 2015). Additional observations were obtained from the $\Delta^{14}C$ measurement programs at the University of Heidelberg (Levin et al., 2023), the University of California, Irvine, and Rafter Radiocarbon Laboratory, Earth Sciences New Zealand (Table S1). The GV+6.1 data product includes CO_2 observations from a global array of sites providing measurements in both discrete flasks and from *in situ* air monitoring from a range of sampling platforms including surface sites, tall towers, ships and aircraft in the NOAA GGGRN and from other laboratories and measurement programs around the world. The locations and numbers of assimilated $\Delta^{14}C$ observations are given in Table S1 for the U.S. and the world, with map locations shown in Figure 1. In contrast to earlier work in which we assimilated only mid-afternoon CO_2 observations from surface sites, here we follow a more comprehensive data selection and representation strategy based on how well the variability of CO_2 at a given site is reproduced by the TM5

https://doi.org/10.5194/egusphere-2026-2896
Preprint. Discussion started: 6 July 2026

transport model run forward with prior fluxes (Jacobson et al., 2023). The effect of this strategy is that data from surface sites are assimilated for most hours of the day, but with elevated *a priori* (assigned) model-data mismatch errors during those times when observations are less well represented, as discussed in the SI. Observations from NOAA's aircraft profiling sites are also assimilated. In the case of $\Delta^{14}CO_2$, most of the observations come from North America, reflecting early NOAA program goals focused on quantifying U.S. $FFCO_2$ emission. Of ~25 ^{14}C sampling sites comprising ~2,035 measurements globally in 2015, 18 are located in North America, comprising 1,615 measurements (respective totals for 2010 are 1,379 and 1,193).

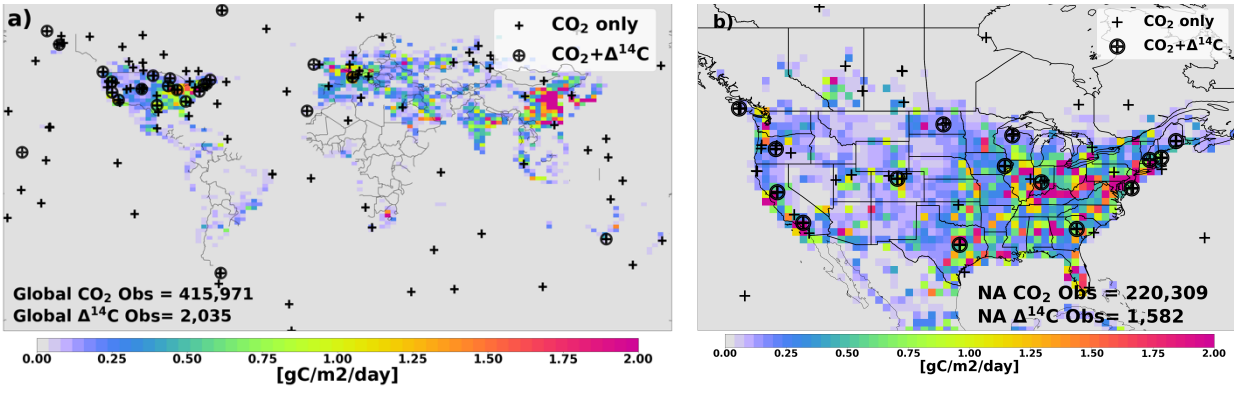

Figure 1: Locations of (a) global and (b) North American (b) observing sites in 2015 providing both CO_2 and $\Delta^{14}CO_2$ measurements (circled plus symbols) and CO_2 measurements only (plus symbols). The pattern of prior mean annual 2015 $FFCO_2$ emission (here, for the example of Miller/CT2022) is also given to illustrate the relationship between the distribution of emissions and observing sites. Measurement counts (including bounding months) are given in the inset of each panel (see text and Table S1 for numbers of assimilated measurements for 2010).

2.3 Prior fluxes and flux optimization

Flux optimizations are conducted using an ensemble of nine priors based on combinations of three fossil and three NBE priors (Sections 2.3.1 and 2.3.2). For all nine flux inversions, we adjust *a priori* fluxes at the grid-scale subject to space-time correlations imposed by B (eq. 1, SI). For both years, our preferred $FFCO_2$ estimates are the mean of the 9-member ensemble, weighted by the estimated posterior uncertainty for each inversion as determined using a Monte Carlo (MC) technique described in Section 2.4. Fossil fuel, net ocean and land fluxes are optimized weekly, while so-called isotopic disequilibrium fluxes (Section 2.3.3) associated with heterotrophic respiration on land and sea-to-air gas transfer over ocean areas are optimized monthly at grid scale. U.S. and global totals for all prior fluxes are itemized in Table S6.

https://doi.org/10.5194/egusphere-2026-2896
Preprint. Discussion started: 6 July 2026

2.3.1 $FFCO_2$

As in the earlier work, we specify different 3 $FFCO_2$ priors, namely those coming from a) the Open-source Data Inventory for Anthropogenic CO_2 (ODIAC, v2022 – ODIAC2022, hereafter "ODIAC") (Oda et al., 2018; Oda and Maksyutov, 2015), b) the Fossil Fuel Data Assimilation System (FFDAS v2, or "FFDAS") (Asefi-Najafabady et al., 2014), and from c) NOAA's CarbonTracker version CT2022 ("Miller/CT2022") (Jacobson et al., 2023), in order to assess system sensitivity to differences in the magnitude, seasonal timing and spatial pattern of prior $FFCO_2$ that may not be captured entirely by prior $FFCO_2$ uncertainties encoded in B (eq. 1 and SI). We also note that the recent update of Miller/CT2016 $FFCO_2$ prior to the current Miller/CT2022 version includes a spatial pattern that differs significantly from the earlier version used in Basu et al., (2020) due to changes to the underlying EDGAR product (Crippa et al., 2019) used to distribute Miller/CarbonTracker fluxes onto a global 1°x1° spatial grid (and aggregated to 3°x2° outside the U.S. 1°x1° zoom region). Grid-wise differences between the two versions of the Miller/CarbonTracker prior for 2010 are shown in Figure S1 and the impact of this revision on the magnitudes and patterns of estimated (posterior) $FFCO_2$ fluxes is discussed in Section 3.4.2.

2.3.2 NBE

As previously shown in Basu et al. (2020), in the limit of relatively few $\Delta^{14}CO_2$ observations, the system may display $FFCO_2$ sensitivity to the choice of prior NBE that can be substantially larger than the derived posterior $FFCO_2$ analytical uncertainty. This likely stems from the inability of the observations to adjust for potentially large differences in the spatial pattern and magnitude of NBE coming from different terrestrial biosphere models used to our inform prior fluxes- i.e., inter-model differences in NBE patterns that are not captured by random perturbation of any single NBE prior alone. The three NBE priors are from a) NOAA's CarbonTracker version CT2016 ("CT16") (Peters et al., 2007, with updates documented at https://carbontracker.noaa.gov), b) NOAA's CarbonTracker version CT2019B posterior NBE ("CT19B") (Jacobson et al., 2020), and c) the Simple Biosphere Model version 4.2 (SiB4) (Haynes et al., 2020). These represent a range of NBE over the U.S. (including AK and HI) of -263 to -111 TgC/yr in 2015 and -343 to -211 TgC/yr in 2010.

2.3.3 ^{14}C specific fluxes

In addition to the dominant influence of ^{14}C-free fossil fluxes, the atmospheric $\Delta^{14}CO_2$ budget is also influenced by other disequilibrium fluxes resulting from differences in the isotopic signature of carbon entering and leaving a reservoir and their corresponding one-way gross mass fluxes. As in previous work, we optimize disequilibrium fluxes associated with heterotrophic respiration and sea-to-air gas exchange. However, the relatively small pure isotopic fluxes of ^{14}C from the nuclear power sector and those from natural cosmogenic production are held fixed at their prior values (Table S6).

https://doi.org/10.5194/egusphere-2026-2896
Preprint. Discussion started: 6 July 2026

2.4 Uncertainty estimation and resolution of derived fluxes

Because the determination of formal analytical uncertainty estimates in the 4DVar optimization scheme requires many more iterations than is computationally feasible, we estimate posterior uncertainties using a MC approach in which observations and prior fluxes are randomly perturbed according to their assigned uncertainties (B and R, respectively, eq. 1) across an ensemble of 100 inversions as in Basu et al. (2020). In addition to the uncertainties obtained from the diagonal of the posterior covariance matrix, $\hat{B}$, we also analyze off-diagonal elements of $\hat{B}$ in order to evaluate the ability of the system to resolve either different flux types (net CO_2 flux, NBE, $FFCO_2$ and disequilibrium fluxes) or individual fluxes between individual U.S. regions (eastern, central and western) or between the U.S. and far-field ocean and land regions, as discussed in Section 3.4.4.

In the current work, we increased the magnitude of *a priori* uncertainties for $FFCO_2$ and terrestrial biological disequilibrium fluxes previously used by Basu et al. (2020) by approximately a factor of two to obtain globally- and regionally-aggregated uncertainties that better reflect overall uncertainties in the atmospheric $\Delta^{14}CO_2$ budget, as summarized in Table S2. As in Basu et al. (2020), the spatial distribution of prior $FFCO_2$ uncertainty scales to the maximum grid-wise differences amongst all three $FFCO_2$ priors, such that B will be the same for each. In the case of NBE, the assigned prior uncertainty is proportional to the associated gross respiration flux (i.e., one of the two primary gross fluxes determining the net flux) such that B is the same for the two CarbonTracker-related priors but is different for the SiB4-based prior. Thus, MC-derived posterior $FFCO_2$ uncertainties for the SiB4-based experiments differ from those for the other six ensemble members (Table 1). Estimated annual and monthly posterior $FFCO_2$ uncertainties are given as either the 1- or 2σ standard deviation of the nine-member ensemble range and are generally larger than the equivalent 1- or 2σ MC based posterior uncertainty estimates representing the random error for any single inversion.

2.5 Impacts of system changes

The combined impact of the system changes (CO_2 ObsPack, Miller/CT2022 $FFCO_2$ spatial pattern, updated prior flux uncertainties, and transport) on the U.S. annual total posterior $FFCO_2$ for 2010 relative to the earlier results of Basu et al. (2020) is +118 TgC/yr. Of that, + 11 TgC/yr is due to the change in prior flux uncertainty and +15 TgC/yr to the change in transport. By far the largest impact arises from the change in the spatial pattern associated with updated Miller/CT2022 $FFCO_2$ prior amounting to +139 TgC/yr, while the change in the CO_2 ObsPack and associated data selection procedures resulted in a change of -47 TgC/yr. The two other $FFCO_2$ priors, FFDAS and ODIAC (Section 2.3.1), have distributions that have not been subject to significant change and their interaction with the updated ObsPack may differ from that when specifying Miller/CT2022. In addition, some $\Delta^{14}C$ measurements from the University of Heidelberg network were excluded from the present study due to suspected measurement biases but have recently been updated (CO2MVS Research on Supplementary Observations (CORSO) project (Levin et al., 2023)). We therefore performed a limited number of experiments that include

https://doi.org/10.5194/egusphere-2026-2896
Preprint. Discussion started: 6 July 2026

the updated data and found little impact on posterior fluxes of $FFCO_2$ and NBE over the U.S. (10 and 9 TgC/yr resp., Tables S3 & S4).

2.6 Additional flux data sets

2.6.1 $FFCO_2$ fluxes reserved for posterior comparison

Derived national and regional annual and monthly total $FFCO_2$ results are compared to values aggregated from the Vulcan 3.0 emissions data product and from the EPA (EPA, 2024b). To enable scientifically meaningful comparison of the inverse and bottom-up results, the latter were adjusted to account for emissions that might be sensed by the atmospheric observing network but which were not included in the Vulcan and EPA products, such as certain emissions from aviation. In the case of Vulcan, a negative adjustment is also applied to account for their inclusion of (non-fossil) emissions from biofuel combustion within the transportation sector. Total monthly and annual adjustments are nonetheless always net positive. Individual adjustments and methods are detailed in Basu et al. (2020) and Table S5.

2.6.2 OCO2 Model Intercomparison Project and TRENDY NBE

We use posterior NBE estimates for the U.S. from the OCO2 v10 Model Intercomparison Project (OCO2 v10 MIP) ensemble (Byrne et al., 2023) and an ensemble of forward estimates from the TRENDY terrestrial biosphere model intercomparison (v9.0) (Sitch et al., 2015) in order to assess the representativeness of the *a priori* NBE ensemble members employed here, which were selected primarily based on ease of access and implementation rather than (assumed) plausibility of their space-time flux characteristics. The OCO2 v10 MIP inversion results were derived from a combination of CO_2 column data retrieved over land and surface-based measurements of CO_2 from both *in situ* sensors and discrete air samples (specifically, the Land Nadir and Land Glint retrievals and in-situ measurements or "LNLGIS" results available at https://gml.noaa.gov/ccgg/OCO2_v10mip/download.php). Results from both the TRENDY and the OCO2 MIPs were screened to eliminate seemingly non-physical representations of NBE seasonality (such as lack of a summertime uptake signal) in order to ease the visual comparison with the priors used in the current work.

3 Results and Discussion

3.1 National and monthly results

Updated monthly U.S. national $FFCO_2$ totals for 2010 and 2015 are shown in Figures 2 and 3 and expressed as their respective 9-member uncertainty-weighted ensemble means and standard deviations (1σ), along with the monthly mean and 1σ spread of the 3 $FFCO_2$ priors and adjusted monthly $FFCO_2$ totals from the Vulcan 3.0 emission data product. Annual total emissions for individual ensemble members for both 2010 and 2015 are given in Table 1 and illustrated in Figs. 4 and 5. Significant positive deviation of the posterior results from their respective priors (and their mean) in all months indicate a statistically robust

https://doi.org/10.5194/egusphere-2026-2896
Preprint. Discussion started: 6 July 2026

adjustment of the $FFCO_2$ priors to larger emissions in response to the assimilated observations. For the annual totals, ensemble spreads are shown and discussed at 2σ to enable more meaningful comparison to the bottom-up data products for which the native uncertainties are expressed as 95% CI. The derived ensemble mean posterior U.S. national $FFCO_2$ for 2010 for the inverse results is 1715 ± 88 TgC/yr while the adjusted Vulcan 3.0 total is 1678 (+279, -235 at 95% CI) TgC/yr, representing agreement to within 2.2 %. For comparison, the agreement between the original three-member ensemble mean annual total for 2010 of Basu et al. (2020) and the similarly-adjusted Vulcan 2010 total (1653 ± 60 TgC/yr) was 1.4%, but the inversion posterior ensemble mean annual total was slightly less than the Vulcan total (Gurney et al., 2020a; Gurney et al., 2020b). As outlined above (Section 2.5), much of the change in the update relative to the original result of Basu et al. (2020) stems from two relatively large, but offsetting effects: 1) the number and weighting of assimilated CO_2 observations, and 2) the revision of the $FFCO_2$ spatial distribution of the Miller/CarbonTracker prior, despite the nearly identical annual national prior totals of 1543 (original) and 1532 (updated) TgC/yr. Although the $FFCO_2$ results for 2010 from Basu et al. (2020) and this study agree to well within their assigned 2σ uncertainties, the updated results and their uncertainties are almost certainly more reliable. For example, the current study makes use of a much larger array of CO_2 observations, which provides improved constraints on the total CO_2 flux in most regions of the U.S., and we now provide a fuller representation of possible *a priori* flux magnitudes and distributions for both NBE and $FFCO_2$ and their uncertainties (i.e., B in eq. 1). In the case of $FFCO_2$ fluxes, the increased uncertainty comes primarily from the update to the Miller/CarbonTracker $FFCO_2$ prior with a spatial distribution that differs substantially from both its earlier version (Fig. S1) and the FFDAS and ODIAC $FFCO_2$ distributions over the U.S., leading to greater per pixel spread (Fig. S2) and spread- derived *a priori* uncertainties. The increased in (primarily) CO_2 observational coverage also led to a significant reduction in the large winter-to-winter (2009/10 vs. 2010/11) $FFCO_2$ difference noted but not resolved in Basu et al. (2020). In the updated results, the winter-to-winter (DJF) difference is substantially smaller (+2.3 ± 0.6% vs. 16 ± 5.0% previously), although it is still of the opposite sense to the winter-to-winter change in emission that might be expected in response to winter time energy use as reflected by the change in the population-weighted number of heating degree days (HDDs) of -2% over the contiguous U.S. (EIA, 2024). Overall, the updated monthly and annual results are in good agreement with those from Vulcan 3.0 (Gurney et al., 2020b; Gurney et al., 2020a) and resolve the expected overall seasonal changes in emissions associated in large part with elevated heating energy demand during wintertime and cooling energy demand in summer.

Figure 3 shows inversion ensemble and adjusted Vulcan results for 2015. To highlight the magnitude and timing of differences between results for 2015 and 2010, we also show the 1σ monthly posterior ensemble spread for 2010. As for 2010, most monthly posterior $FFCCO_2$ results in 2015 are significantly larger than the associated monthly mean priors, with the exception of May through August. The smaller mean adjustment in this period results almost entirely from posterior $FFCO_2$ fluxes associated with the three ensemble members utilizing the SiB4 NBE prior (Fig. 5), which in 2015 displays net biosphere summertime uptake significantly greater than in other models (Fig. S4). Given some degree of total carbon constraint from the many CO_2 observations, the large magnitude of anomalous NBE uptake in the prior may lead to some aliasing of the required

https://doi.org/10.5194/egusphere-2026-2896
Preprint. Discussion started: 6 July 2026

total CO_2 adjustment into the derived posterior $FFCO_2$ signal. For example, annualized mean May-August NBE in the SiB4 prior is -4428 TgC/yr vs. -3094 TgC/yr for the OCO2 v10 MIP ensemble mean, a difference of -1334 TgC/yr that is almost as large as the annualized mean May-August prior $FFCO_2$ flux of 1421 TgC/yr. In the limit of relatively few $\Delta^{14}CO_2$ observations discriminating between NBE and $FFCO_2$ fluxes in any given month, aliasing of such a large "anomalous" prior NBE flux into the posterior $FFCO_2$ estimate is not surprising.

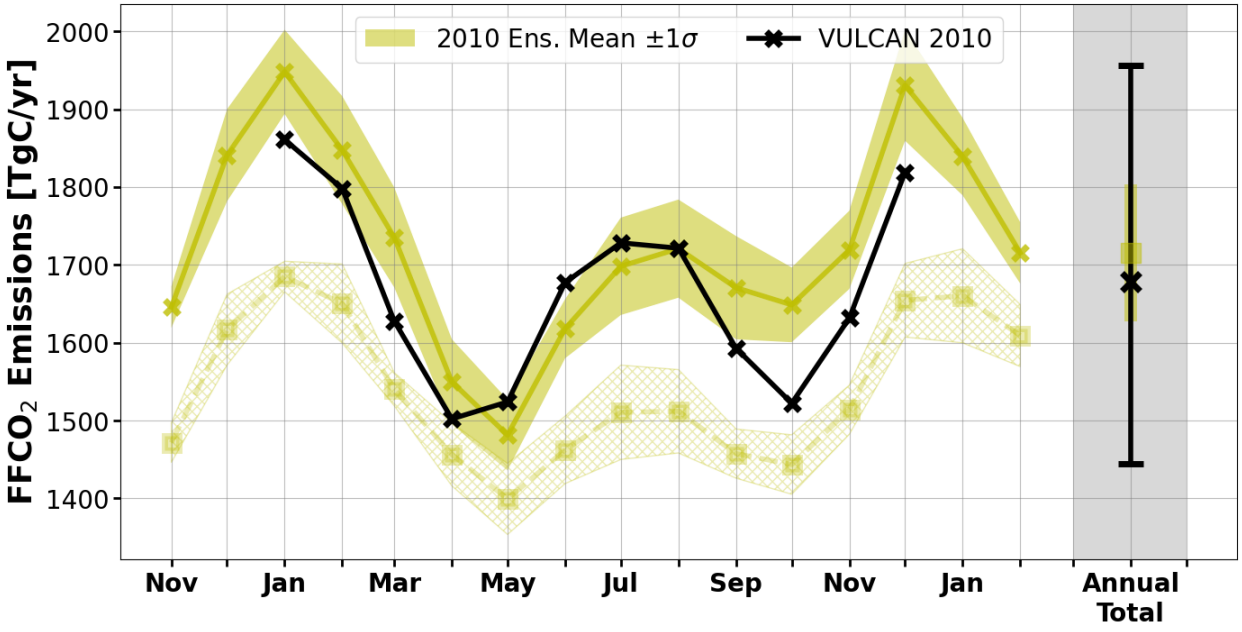

Figure 2: Monthly 9-member uncertainty-weighted ensemble mean posterior $FFCO_2$ totals (solid yellow line) for the U.S. (including Alaska and Hawaii) for 2010, along with their uncertainty-weighted ensemble-wide 1σ ranges (yellow shaded envelope). The corresponding mean $FFCO_2$ prior and 1σ ranges are given by the dashed yellow line and hatched envelope, respectively. Results for the two bounding months before and after of 2010 are also included. The black solid line denotes monthly adjusted $FFCO_2$ totals from the U.S. specific Vulcan emissions data product (Gurney et al., 2020). Uncertainty-weighted ensemble-mean annual totals and their 2σ ensemble-wide range are given in the gray panel along with the Vulcan annual total and its associated 95% confidence interval. Small adjustments to Vulcan follow those of Basu et al. (2020) and are discussed in the text.

https://doi.org/10.5194/egusphere-2026-2896
Preprint. Discussion started: 6 July 2026

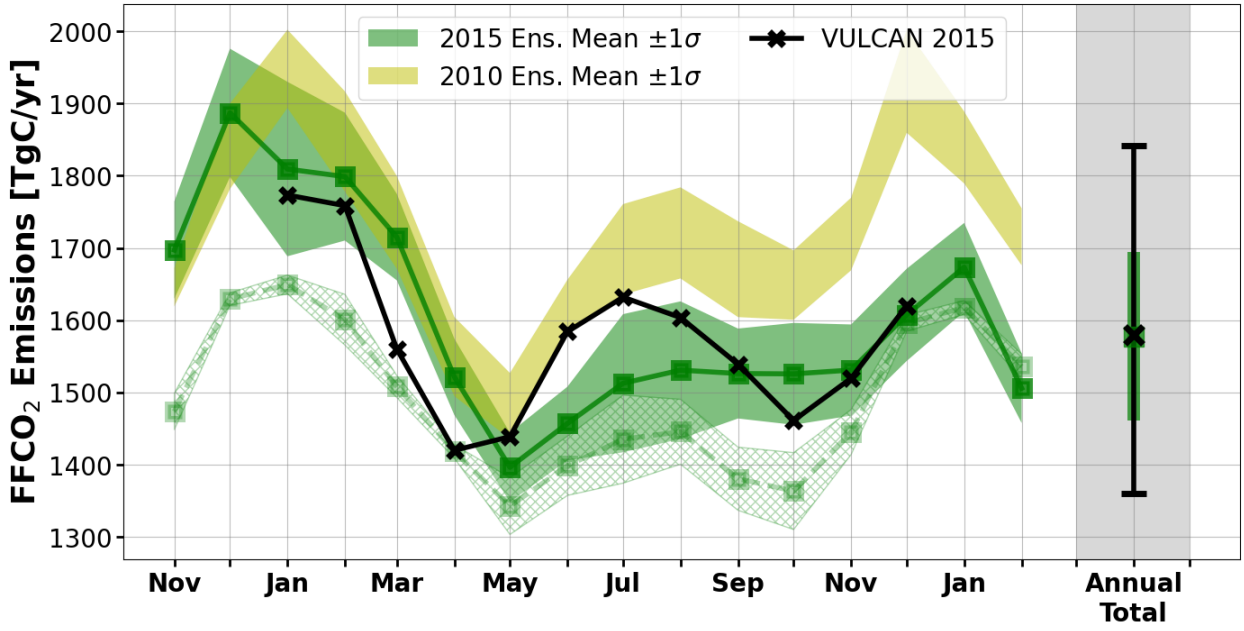

Figure 3: Same as Fig. 2, but for 2015 (green). To highlight differences between 2015 and 2010, the 1σ ensemble-wide range of monthly fluxes for 2010 is show in yellow (per Fig. 2).

As in 2010, for 2015, we again see annual ensemble mean annual total emissions that agree with adjusted totals from Vulcan 3.0; 1578 TgC/yr (±116 TgC/yr at 2σ) for the inversions and 1580 TgC/yr (+262 and -221 TgC/yr at the 95% CI range) for Vulcan (Table 1). Also notable in the inverse results is the fact that much of the reduction in $FFCO_2$ between 2010 and 2015 of -135 TgC/yr (±26 TgC/y) occurred during the latter half of 2015 (Fig. 3). This is also evident when comparing monthly Vulcan results for the two years (and is true of both adjusted and unadjusted Vulcan values). Posterior wintertime differences between 2010 and 2015 are also consistent with expected $FFCO_2$ emission changes associated with differences in wintertime heating demand. The number of population-weighted HDDs in the winters of 2009/10 and 2014/15 (2608 and 2486, resp.) are similar, while 2010/11 vs. 2015/16 population-weighted HDDs are substantially different (2667 and 2105, resp.) (EIA, 2024), in broad agreement with the inverse estimates.

https://doi.org/10.5194/egusphere-2026-2896
Preprint. Discussion started: 6 July 2026

Table 1: Estimated U.S. National $FFCO_2$ emissions for each of nine ensemble members for 2010 and 2015 along with their formally-derived 1σ uncertainties and the uncertainty-weighted ensemble-wide mean and 2σ range for each year. Associated inter-year differences and their quadrature sum uncertainties for all estimates are also shown. Prior emissions and their inter-year difference and adjusted national totals for the Vulcan emissions data product (Gurney et al., 2020a; Gurney et al., 2020b) and from the EPA (EPA, 2024a) are given for comparison. Although inter-year differences for Vulcan and EPA would not appear to be significant at their respective 95% CIs, these almost certainly reflect systematic rather than random uncertainties. Thus, inter-year differences may be more robust than central single year estimates.

	2010 (TgC/yr)		**2015 (TgC/yr)**		**2010- 2015 (TgC/yr) (*prior diff.*)**	**-% Diff.**
Experiment (prior FF/NBE)	**$FFCO_2$ (*prior*)**	**unc.**	**$FFCO_2$ (*prior*)**	**unc.**		
Miller/CT16	1745 (*1532*)	26	1581 (*1465*)	29	164±40 (*67*)	9.4
FFDAS/CT16	1653 (*1485*)	26	1486 (*1433*)	29	167±40 (*52*)	10.1
ODIAC/CT16	1690 (*1552*)	26	1525 (*1496*)	29	165±40 (*56*)	9.8
Miller/CT19B	1791	26	1681	29	110±40	6.1
FFDAS/CT19B	1701	26	1588	29	112±40	6.6
ODIAC/CT19B	1735	26	1626	29	109±40	6.3
Miller/SiB4	1729	49	1610	37	120±64	6.9
FFDAS/SiB4	1655	49	1528	37	127±64	7.7
ODIAC/SiB4	1684	49	1565	37	120±64	7.1
Unc. weighted mean and 2σ range	**1715±88**	…	**1578±116**	…	**135±52**	**7.8**
Vulcan [95% CI +/-]	**1678 [279/235]**	…	**1580 [262/221]**	…	**98**	**5.8**
EPA [95% CI +/-]	**1575 [64/32]**	…	**1494 [60/30]**	…	**81**	**5.1**

Although derived annual mean ensemble-wide $FFCO_2$ totals and adjusted Vulcan totals are very similar for both 2010 and 2015, there are notable differences in the magnitude of associated monthly totals (Figs. 2 and 3). In addition to the suppression of the expected secondary summertime emissions maximum associated with cooling energy demand mentioned above, all three 2015 NBE ensemble sets (each associated with three $FFCO_2$ priors) and their uncertainty weighted-means depict a later winter-to-summer $FFCO_2$ decline and a later spring-time minimum than Vulcan (Fig. 5). This is also evident, but to a lesser extent, in 2010 (Fig. 4). It is important to note that we expect derived annual totals to be more reliable than individual monthly totals. This likely results primarily from two factors. First, as noted above, in the current case the number of $\Delta^{14}CO_2$

https://doi.org/10.5194/egusphere-2026-2896
Preprint. Discussion started: 6 July 2026

345 observations over the U.S. in any single month is quite small (typically, ~80). Second, adjustments to the underlying prior $FFCO_2$ fluxes have an assigned a temporal correlation e-folding time-scale of 3 months, limiting the degree of independent $FFCO_2$ flux adjustment in any single month. (The sensitivity of results to alternate specifications of temporal and spatial correlation length is discussed in Section 3.4.3.) Indeed, a comparison of 3-month ensemble means from the inversions and from Vulcan agree to within 1σ for 7 of 10 3-month intervals across both 2010 and 2015 inversions, and well within 2σ for the
350 remaining 3 (Table 2). Given the relative paucity of $\Delta^{14}CO_2$ observations in any single month, the recovery of a realistic seasonal cycle was not entirely expected (c.f. Basu et al. (2016)) and points to the strong sensitivity of $\Delta^{14}CO_2$ to $FFCO_2$ emissions and a relative insensitivity to any remaining uncertainties in other $\Delta^{14}CO_2$ budget terms over North America.

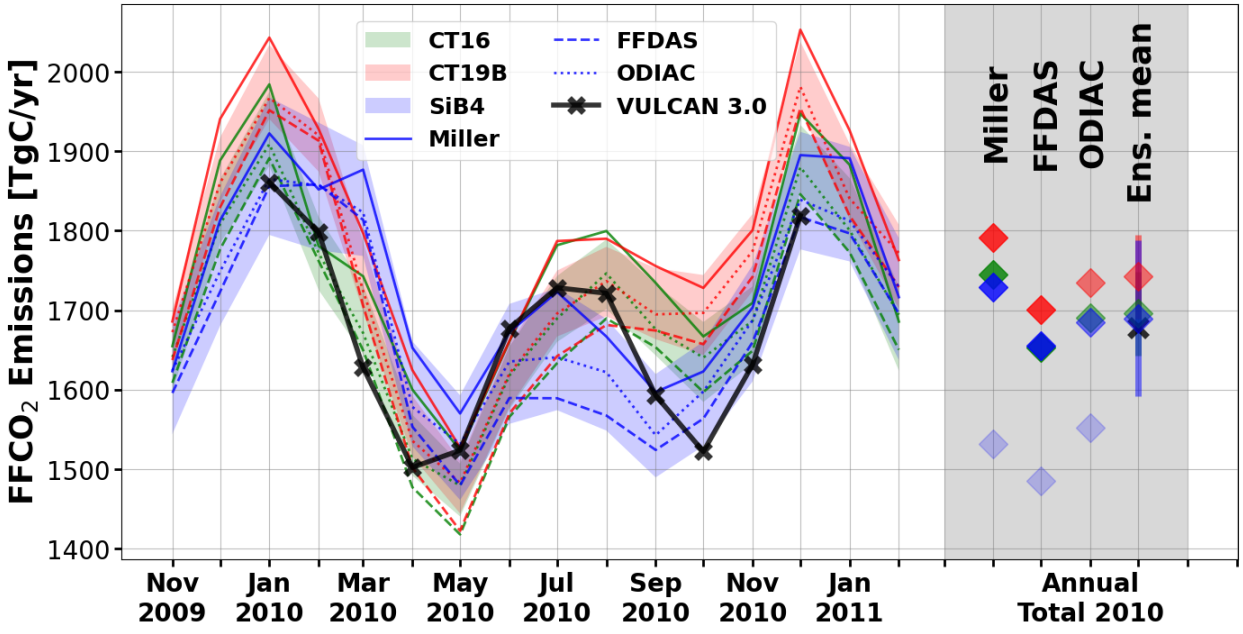

355

Figure 4: Monthly and annual posterior U.S. $FFCO_2$ fluxes for 2010 (and bounding months) for all 9 ensemble members (see Table 3), grouped by the choice of NBE prior, as discussed in the main text. Shaded envelopes denote the 1σ analytical uncertainty with respect to the 3-member mean (not shown) for each NBE-based 3-member grouping. Respective annual totals for each prior $FFCO_2$:NBE pair are given in the gray shaded region along with uncertainty-weighted ensemble mean $FFCO_2$
360 totals and 2σ ranges for each 3-member grouping. Adjusted Vulcan monthly and annual totals are also shown for reference (as in Fig. 2.).

https://doi.org/10.5194/egusphere-2026-2896
Preprint. Discussion started: 6 July 2026

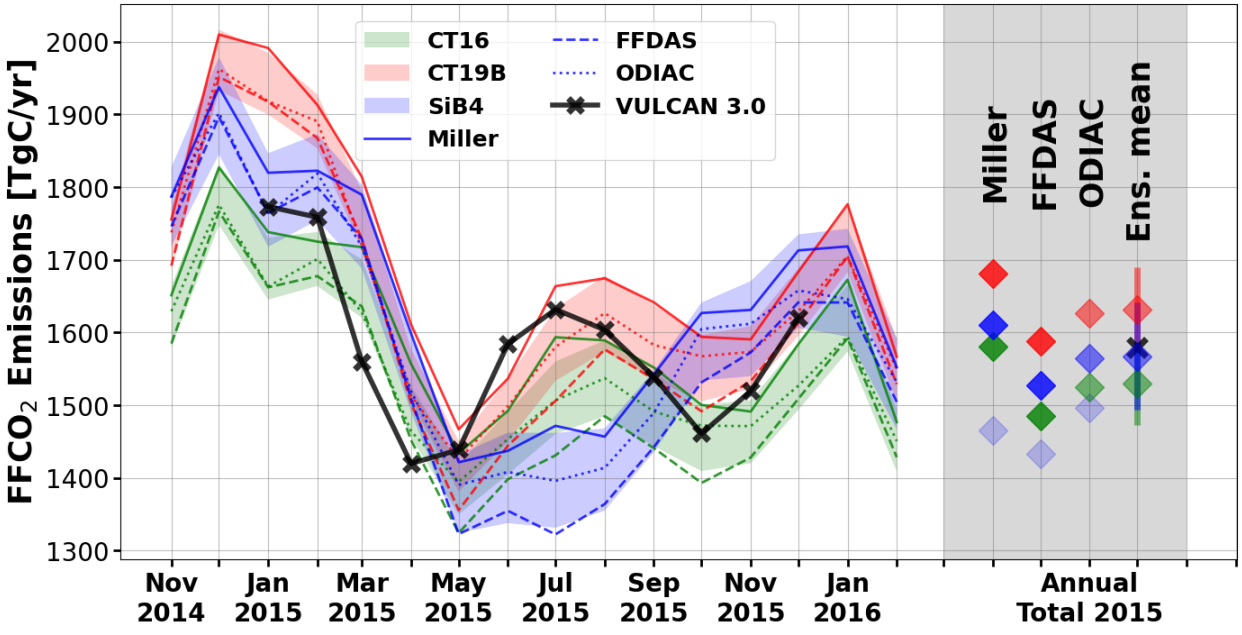

Figure 5: Same as Fig. 4 but for 2015.

Table 2: Comparison of uncertainty-weighted ensemble-wide mean national $FFCO_2$ totals and uncertainties compared to adjusted Vulcan U.S. National $FFCO_2$ totals for 5 tri-monthly periods in 2010 and 2015. Italicized entries differ by more than the 1σ ensemble-wide range.

	2010 (TgC/yr)			2015 (TgC/yr)		
	ensemble	**unc.**	**Vulcan**	**ensemble**	**unc.**	**Vulcan**
DJF	464	13	451	452	24	431
MAM	401	13	392	*389*	*13*	*371*
JJA	423	13	432	*378*	*20*	*405*
SON	*419*	*13*	*395*	381	15	376
DJF	452	12	444	398	14	405

3.2 Inter-year differences

Figure 6 compares ^{14}C-derived annual $FFCO_2$ totals and their estimated uncertainties (i.e., 2σ ensemble-wide spreads) to adjusted results from the Vulcan 3.0 emissions data product and the U.S. EPA (EPA, 2024b) along with their estimated 95% CIs. Results from Vulcan and the EPA are also given for intervening years in order to provide an impression of possible inter-annual variability and trend of U.S. $FFCO_2$ over the interval. Posterior ensemble-mean $FFCO_2$ fluxes for the U.S. were 1715 ± 88 Tg C/yr in 2010 and 1578 ± 116 TgC/yr (both at 2σ) in 2015, amounting to an inter-year reduction of 135 ±52 TgC/yr or

https://doi.org/10.5194/egusphere-2026-2896
Preprint. Discussion started: 6 July 2026

7.8 ±3.0 % (both at 2σ). Each of the year-vs.-year ensemble pairs (i.e., prior $FFCO_2$ and NBE pairs) also indicate a reduction in derived national total $FFCO_2$ between 2010 and 2015 that range from 6.1% to 10.1% (Table 1). Moreover, the year-vs.-year difference amongst the three prior $FFCO_2$ emissions estimates is only -3.8 ± 0.4%, indicating that the differences between posterior estimates are being driven largely by signals in the atmospheric observations.

As noted above, ^{14}C-based and adjusted Vulcan 3.0 totals agree to well within the derived ensemble spreads in both 2010 and 2015 and inter-year differences for the two are therefore also similar, with central estimates from Vulcan indicating a reduction of 98 TgC/yr, or 5.8% (and 95 TgC/yr or 5.8% for unadjusted totals) (Table 1). Geographically comparable national totals from the EPA for 2010 and 2015 overlap the ^{14}C-derived estimates within their given uncertainties, with an associated inter-year difference of 81 TgC/yr (+4, -2 at 95% CI) or 5.1 % (+0.25, -0.13 at 95% CI). Thus, the atmosphere-based estimates of the change in U.S. $FFCO_2$ emission between 2010 and 2015 are consistent with estimates reported by Vulcan and the EPA, with central estimates that range from -7.8% to -5.1%. The EPA identifies multiple factors contributing to decreasing $FFCO_2$ emission during this period, including ongoing replacement of coal with natural gas for electricity generation, decreases in overall electricity demand, and warm winter conditions in 2015/16 that lead to a reduction in demand for heating in the residential and commercial sectors (EPA, 2024a). Likewise, Gurney et al. (2020b) point to reductions in electricity demand and increases in thermal efficiency (i.e., use of natural gas vs. coal) as primary drivers of the estimated decline in $FFCO_2$ emission between 2010 and 2015.

https://doi.org/10.5194/egusphere-2026-2896
Preprint. Discussion started: 6 July 2026

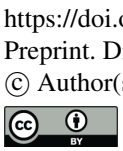

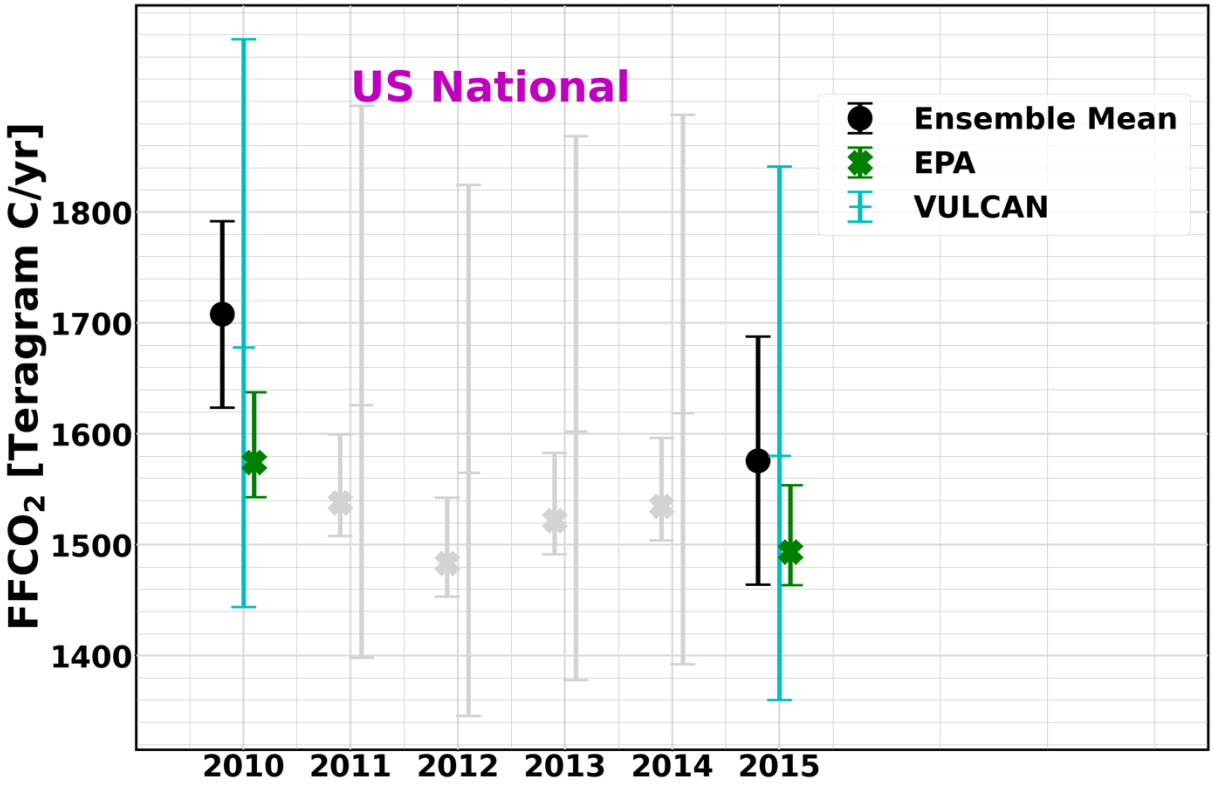

Figure 6: Annual U.S. uncertainty-weighted ensemble-mean $FFCO_2$ totals and their ensemble-wide 2σ range for 2010 and 2015, compared to adjusted totals from the U.S.-specific Vulcan emissions data product (Gurney et al., 2020) and the EPA, both with their respective 95% CIs. Adjusted Vulcan and EPA totals are also shown for 2011-14 (gray symbols), to give an impression of the possible trend and inter-annual variation of emissions. Adjustments to EPA and Vulcan fluxes needed for scientifically meaningful comparison to atmospheric observations are discussed in Section 2.6.1. and itemized in Table S5.

Although individual annual totals are statistically indistinguishable across all three sets of estimates, adjusted EPA totals are lower than the atmosphere-based results and the central estimates from Vulcan in both 2010 and 2015 and, also, consistently lower than Vulcan during the intervening years. Possible sources of systematic differences between Vulcan and EPA estimates have been discussed in some detail by Kato et al. (2023). We note here that, given sufficient density of observations in both space and time, atmosphere-based methods are expected to sense all possible emissions, with uncertainties that stem largely from possible biases in simulated atmospheric transport (Basu et al., 2020; Basu et al., 2016), while bottom-up estimates implicitly require perfect knowledge of all possible emission sources and their intensities. It is therefore not surprising that our

https://doi.org/10.5194/egusphere-2026-2896
Preprint. Discussion started: 6 July 2026

atmosphere-based $FFCO_2$ emissions estimates are larger than most bottom-up estimates, including all three prior $FFCO_2$ estimates employed in this study (i.e., Figs. 2-5). Strong agreement between our atmosphere-based estimates and Vulcan suggests that, unlike many global products, the U.S. specific Vulcan data product captures the majority of all true U.S. emissions (with the deliberate exception of certain aviation emissions, Table S5). And, given what appears here to be a consensus decrease in $FFCO_2$ emission of 8% to 5% between 2010 and 2015, it seems likely that provisional uncertainty estimates for the Vulcan 3.0 emissions data product of -14% and +16% (95% CI) may be much larger than warranted.

3.3 Regional results and resolution

In addition to national totals, for both 2010 and 2015, we summed posterior 1˚x1˚ fluxes to calculate $FFCO_2$ emissions for three large U.S. subregions - west, central and east (Fig. S7). Regional ensemble-mean totals and their uncertainty-weighted 2σ ranges are given in Table 3 along with adjusted Vulcan 3.0 and EPA totals. The regional estimates for EPA were derived by aggregating all state fluxes falling inside each region using EPA state level data (EPA, 2024b). Similarly, nationally gridded Vulcan estimates were aggregated within regional boundaries. In both cases, regional totals were adjusted by applying nationally-derived adjustment factors given in Table S5 and discussed in Basu et al. (2020).

Estimates of regional emissions for the inversions and from the bottom-up estimates are in broad agreement, with the exception of the Western U.S. in both years, where the inverse estimates differ from either or both Vulcan and EPA by more than 2σ (italicized entries in Table 3). In both 2010 and 2015, the inverse results show that the eastern region of the U.S. is by far the largest source of fossil CO_2 emissions, representing 52% (2010) and 49% (2015) of the national total, slightly less than proportions based on estimates from Vulcan (57% and 56%, for 2010 and 2015, resp.) and EPA (55% and 53%). In the inverse results, the rank order of ensemble-mean emissions estimates for the western and central U.S. differs between 2010 and 2015, although absolute emissions for the two regions overlap at their respective 2σ ensemble ranges in both years. In contrast, the EPA and Vulcan indicate emissions in the central U.S. are consistently larger than those in the western U.S. (+10% and +6% in 2010 and 2015, resp.), although uncertainties for regionally aggregated EPA and Vulcan emissions are not readily available.

The ^{14}C-based results and the EPA and Vulcan bottom-up products all suggest that reductions in national-scale emissions between 2010 and 2015 are dominated by reductions in the eastern U.S. (Table 3). Relative reductions in this region between 2010 and 2015 represent 91%, 93% and 80% of the national decline for the three sets of estimates, respectively. Such regional dominance of the overall U.S. decline is expected, given the large presence of electric power plants in the eastern U.S. (~65 % of total U.S. power generation according to https://www.eia.gov/electricity/data/state/), many of which transitioned from coal to less carbon-intensive natural gas combustion during this period (EPA, 2024a). In both the western and central U.S., the inverse estimates for 2010 and 2015 differ by less than 2σ while derived inter-year differences for Vulcan and EPA are small (ranging from 0 to 13 TgC/yr), but of undetermined statistical significance.

https://doi.org/10.5194/egusphere-2026-2896
Preprint. Discussion started: 6 July 2026

Table 3: U.S. national and regional uncertainty-weighted ensemble-mean totals and ensemble-wide ranges (2$\boldsymbol{\sigma}$) along with adjusted Vulcan and EPA totals for 2010 and 2015 and associated inter-year differences. Italicized entries denote values that differ between the inverse estimates and those from either Vulcan or the EPA by more than 2$\boldsymbol{\sigma}$.

Region	2010 $FFCO_2$ (TgC/yr)			2015 $FFCO_2$ (TgC/yr)			Difference (TgC/yr)		
							Ens.	Vulcan	EPA
	Ens.	**Vulcan**	**EPA**	**Ens.**	**Vulcan**	**EPA**			
U.S.	1715±88	1678 [+279/ -235]	1575 [+64/ -32]	1578±116	1580 [+262/ -221]	1494 [+60/ -30]	135±52	98	81
Western U.S.	*445±66*	*311*	*277*	*372±82*	304	*270*	*75*±32	7	7
Central U.S.	381±52	410	434	438±66	397	434	*-63*±14	13	0
Eastern U.S.	895±50	957	864	770±48	879	789	122±18	78	75

Overall, the relatively large ensemble ranges for the western and central U.S. (~±18% and ±14%, resp., when averaged over the two years) indicate that our current observing network is unable to determine fluxes from these regions with the same relative precision as within the Eastern U.S., where the 2σ ensemble range is just ~6%. This most likely results from our early programmatic choice to focus $\Delta^{14}CO_2$ measurement sites within and downstream of this region with the largest expected emissions and the fact that upwind observations in the western and central U.S. provide additional constraints on the composition of "background" air entering the eastern U.S. It is notable, however, that MC ensemble-derived posterior $FFCO_2$ fluxes amongst the different (even adjacent) U.S. regions are largely uncorrelated (Table 5), indicating that the inversion system is able to independently resolve and constrain $FFCO_2$ in the different regions, as discussed in detail below in Section 3.4.4. This underscores an important distinction between regional flux uncertainty and regional flux resolution. We simply add here that the similarity in the sum of Western and Central U.S. fluxes for the inverse results and from EPA and Vulcan arises from the fact that U.S. national and Eastern U.S. totals are similar for all three and, in the inverse results, the associated posterior uncertainties on the national and Eastern U.S. totals are both relatively small. Thus, there is a closed-sum constraint requiring the sum of emissions in remaining (i.e., Western plus Central) regions to be similar across all three estimates. On the other hand, the absence of significant correlation of posterior flux estimates between regions discussed in Section 3.4.4 suggest that the fact that sum of the Western and Central U.S. totals is conserved is not an artifact of unresolved "smearing" of derived emissions between the two regions that might arise from inadequacies of the system transport and observational coverage.

https://doi.org/10.5194/egusphere-2026-2896
Preprint. Discussion started: 6 July 2026

3.4 Evaluation and performance

3.4.1 Representation of observations

To evaluate the performance of the inversion system, we compare simulated CO_2 and $\Delta^{14}CO_2$ for both prior and posterior (optimized) fluxes with actual measurement values used as constraints, both globally and for the U.S. alone (i.e., within the 1°x1° zoom region). Given that the goal of the system is to adjust prior fluxes in order to (once transported) improve the overall fit to the atmospheric observations, we expect posterior simulated CO_2 and $\Delta^{14}CO_2$ values to exhibit better agreement with observations than simulated CO_2 and $\Delta^{14}C$ derived from prior fluxes. The accuracy and precision of the simulations are quantified by calculating the mean and standard deviation (std. dev.) of the residuals which indicate model bias and noise, respectively. Globally, the prior mean bias and std. dev. (1σ) of CO_2 improves from 1.18 ± 3.73 ppm to a posterior value of -0.03 ± 2.79 ppm (Fig. 7a) and from 1.45 ± 4.28 ppm to 0.00 ± 3.34 ppm over the U.S. zoom region (Fig. 7c). A reduction in both bias and noise is also seen for $\Delta^{14}C$, from 0.62 ± 1.68 per mil (‰) to 0.04 ± 1.41 ‰ globally (Fig. 7b) and from 0.60 ± 1.85 ‰ to 0.05 ± 1.54 ‰ over the U.S. (Fig. 7d). For $\Delta^{14}CO_2$, the fact that the initial bias associated with *a priori* fluxes is so small is consistent with earlier forward modeling work using similarly formulated fluxes and transport demonstrating an ability to represent a large global array of observations across the decade of the 2000s (Miller et al., 2025a; Miller et al., 2025b). The relatively modest reduction in noise following flux optimization likely results from the relatively large $\Delta^{14}CO_2$ measurement uncertainty of ~1.8 ‰ (compared to that for CO_2 of ~ 0.2 ppm) which may limit the ability of the model to more precisely represent the observations, even within the higher-resolution U.S. zoom region.

We also evaluated the fit of posterior CO_2 values to observed vertical profiles obtained from individual NOAA aircraft profiling sites over North America, analyzed by season (Figure 8). Individual seasonal mean profiles for both simulated and observed values were normalized to mean simulated or observed CO_2 mole fractions above 5 km above sea level (km asl) in the well-mixed free troposphere, relatively distant from the direct influence of surface exchange fluxes and emissions. With the exception of THD (Trinidad Head, CA) in Fall ("SON"), the simulations closely match observed vertical gradients at all sites and seasons, including strong negative near-surface (i.e., CO_2 declining with height) gradients during Fall and Winter ("DJF") associated with net respiration, enhanced $FFCO_2$ emission and boundary layer "trapping" and, in summer ("JJA"), strong positive near-surface gradients arising from strong net biospheric uptake at that time. Because only surface fluxes are optimized, the ability of the simulation to fit the seasonally-varying vertical structure of the profiles suggests that the vertical component of the atmospheric transport employed here closely approximates the true transport. This in turn suggests that any biases in derived fluxes arising from persistent seasonal bias in the simulated vertical transport (excessive or inadequate vertical mixing resulting in excessive or inadequate dilution of fluxes) over the U.S. domain are correspondingly modest. The poor fit at THD during the Fall likely results from the inability of the model to capture sub-grid-scale changes in land-sea breezes at this coastal site (see Fig. S7 for a map of sites in Fig. 8).

https://doi.org/10.5194/egusphere-2026-2896
Preprint. Discussion started: 6 July 2026

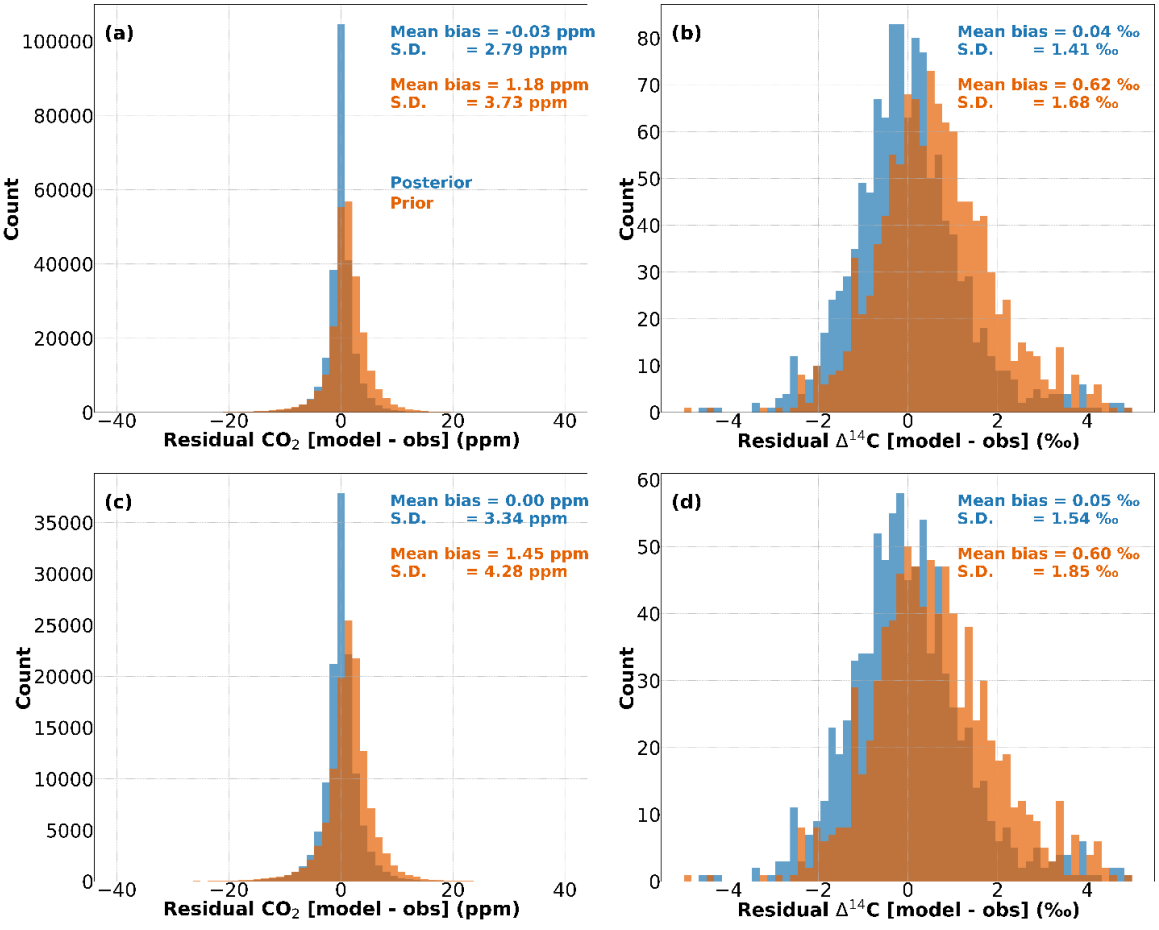

Figure 7: Distribution of CO_2 (left) and $\Delta^{14}CO_2$ (right) residuals (model-observations) before (red) and after (blue) optimization for the full, global set of assimilated observations (upper row) and for the U.S. alone (lower row), for 2015. The mean bias and standard deviation (1σ) of residuals is also given.

https://doi.org/10.5194/egusphere-2026-2896
Preprint. Discussion started: 6 July 2026

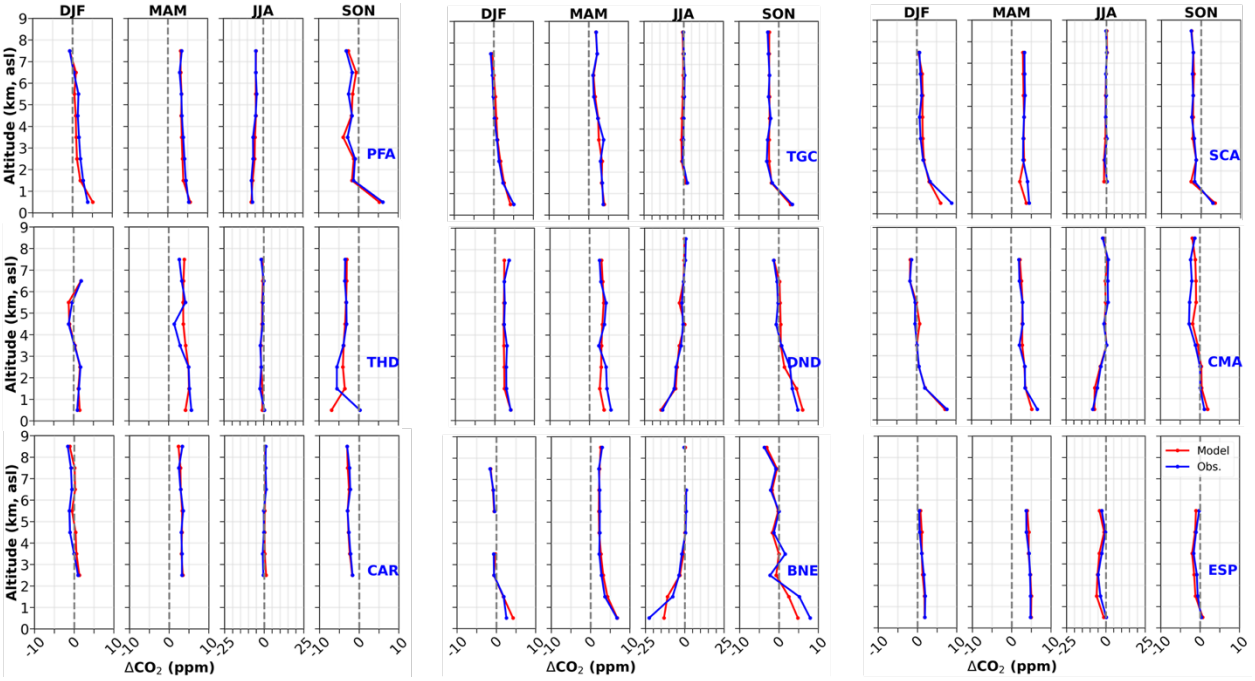

Figure 8: Simulated seasonal mean vertical profiles for 9 North American aircraft profiling sites (red) compared to observations (blue) for Dec. 2009 - Nov. 2010. Simulated and observed profiles are expressed as deviations from mean simulated or observed CO_2 mole fractions above 5 km asl, as discussed in the text. Locations of individual sites are given in Fig. S7. Note that the CO_2 mole fraction scale for JJA is ±25 ppm (vs. ±10 for other seasons), as needed to capture large positive near-surface gradients at some sites at that time. Only results for the first winter (DJF) of the 15 month simulation period are shown, but the model fit to observations for the second winter is similar to results for the first winter at all sites. The number of observations compared to simulated values for individual seasonal profiles ranges from 75-25 (at 1σ) with the low end due primarily to less frequent sampling at THD (1σ range of 24-11).

3.4.2 Sensitivity to $FFCO_2$ and NBE priors

Figures 4 and 5 show derived monthly and annual $FFCO_2$ fluxes for each of the nine (i.e., 3 $FFCO_2$ x 3 NBE) *a priori* flux pairs comprising the experimental ensembles for 2010 and 2015, respectively. Monthly MC-based posterior uncertainties (Section 2.4) are also shown for each common NBE ensemble, centered around the respective ensemble mean, along with ensemble-wide mean uncertainty-weighted annual totals.

https://doi.org/10.5194/egusphere-2026-2896
Preprint. Discussion started: 6 July 2026

For 2010, the impacts of *a priori* $FFCO_2$ and NBE on derived national total $FFCO_2$ (Table 4) are comparable, with standard deviations ranging from 37.3 to 46.3 TgC/yr due to specified *a priori* $FFCO_2$ and from 27.2 to 32.2 to TgC/yr due to *a priori* NBE. For 2015, the differences in sensitivity are greater, with standard deviations ranging from 50.9 to 51.4 TgC/yr due to *a priori* NBE and from 41.1 to 47.8 due to *a priori* $FFCO_2$. In both years, the impact on spread due to *a prior* $FFCO_2$ is increased significantly by the inclusion of the updated Miller/CT2022 prior (Table 4), likely because of a significant change in the spatial pattern of emission compared to the earlier version (Section 2.3.1 and Fig. S1) and to that for the other two priors (see 2015 example in Fig. S2). In contrast to the other priors, although total emissions are similar, the updated Miller/CT2022 prior allocates significantly greater emission to the western half of the country (Figs. S1 and S2). Given that the inversion produces a downward adjustment of *a priori* fluxes for Miller/CT2022 to yield patterns more similar to those for the FFDAS and ODIAC priors in this region (Fig. S3), the Miller/CT2022 prior may be spatially biased. However, the relative paucity of observations within the region and the overall lack of upwind constraints (i.e., over the North Pacific Ocean) likely limit the ability of the inversion system to correct for the apparent regional bias in its entirety. Thus, associated posterior $FFCO_2$ fluxes are higher in this region than for the other two $FFCO_2$ flux priors, leading to larger national totals in both years. As we cannot objectively discard the updated Miller/CT2022 prior (and, implicitly, the updated EDGAR product on which the spatial pattern is based (i.e., Crippa et al. (2019)), we retain the associated posterior estimates in our determination of ensemble-wide mean emissions and their spread. Thus, derived 9-member ensemble-wide 1σ and 2σ spreads likely represent conservative estimates of overall $FFCO_2$ uncertainty.

For each NBE ensemble, derived posterior monthly fluxes associated with each of three $FFCO_2$ priors typically fall within the derived monthly 1σ posterior uncertainty envelope (Figs. 4 and 5), indicating that the estimate of random *a posteriori* uncertainty adequately captures real differences amongst specified $FFCO_2$ priors, as expected (given methods in Section 2.4). However, the fact that the uncertainty envelopes associated with each NBE ensemble exhibit less overlap reflects sensitivity to *a priori* NBE at the monthly scale that is not entirely captured by the overall *a posteriori* uncertainty estimates. As discussed in Basu et al. (2020), this arises in part from the inability of specified prior NBE covariances to represent all systematic differences amongst the selected NBE priors.

The lack of posterior $FFCO_2$ overlap across NBE ensembles is most notable in both years during the summer, when the magnitude of NBE is largest and *a priori* NBE estimates exhibit the most spread, which stems largely from inclusion of the SiB4-based product (Fig. S4). SiB4 also appears anomalous with respect to the fuller range of possible representations of NBE obtained from TRENDY (available for both 2010 and 2015) and the OCO-2 MIPs (available for 2015 only) (Section 2.6.2, Fig. S4). As discussed in Section 3, we suspect that the deviation of $FFCO_2$ results associated with the SiB4 prior results from the inability of the inversion system to correct for an anomalously large *a priori* summertime uptake signal and its subsequent

https://doi.org/10.5194/egusphere-2026-2896
Preprint. Discussion started: 6 July 2026

aliasing into the posterior $FFCO_2$ results. In theory, such aliasing can be overcome by increasing the number of ^{14}C observations in order to better separate $FFCO_2$ and NBE related CO_2 signals (Basu et al., 2016).

Table 4: Impact of choice of NBE prior (rows) or $FFCO_2$ prior (columns) on sub-ensemble mean and standard deviation (1σ). Italicized entries are for NBE-related standard deviation after exclusion of the experiments using Miller/CT2022 as $FFCO_2$ prior, as discussed in the text.

	2010					**2015**				
	CT16	**CT19B**	**SiB4**	**Mean**	**1σ**	**CT16**	**CT19B**	**SiB4**	**Mean**	**1σ**
Miller/CT2022	1745	1791	1729	**1755**	**32.2**	1581	1681	1610	**1624**	**51.4**
FFDAS	1653	1701	1655	**1670**	**27.2**	1486	1588	1528	**1534**	**51.3**
ODIAC	1690	1735	1684	**1703**	**27.9**	1525	1626	1565	**1572**	**50.9**
Mean	1696	1742	1689			1531	1632	1568		
1σ	**46.3**	**45.4**	**37.3**			**47.8**	**46.8**	**41.1**		
w/o Miller/CT2022	***26.2***	***24.0***	***20.5***			***27.6***	***26.9***	***26.2***		

3.4.3 Sensitivity to spatiotemporal length scales of *a priori* flux adjustment

A detailed description of how we construct the prior error covariance structure (*B* in eq. 1) is provided in the supplemental information. Briefly, as is typical for inversions that solve for grid-scale fluxes (Basu et al., 2016), we impose exponentially decaying spatial and temporal error correlations that constrain the relative adjustment to *a priori* fluxes separated by a given distance and time. To evaluate the sensitivity of derived *a posteriori* $FFCO_2$ fluxes to the treatment of prior error correlations, we performed three experiments. In experiment ST1, we replaced the default "hybrid" correlation approach for $FFCO_2$ (see SI and Basu et al. (2016)) with a continuously varying exponential decay function commonly applied in single tracer systems. In experiment ST2 we changed the temporal error correlation length from three months to one month. And in experiment ST3, we increased the spatial error correlation length from 200 km to 500 km for NBE only ($FFCO_2$ was treated as in the default set up). All three experiments were performed for 2015 only, using updated Miller/CT2022 fossil emissions and CT2016 NBE as priors.

The change from default hybrid to a continuously varying exponential error covariance scheme (exp. ST1) led to a reduction in derived annual, national $FFCO_2$ emissions of 26 TgC/yr, or 1.6%, with spatial changes in flux distribution characterized mainly by reductions in the Northeast (Fig. S5). Abbreviation of the temporal length scale of prior error correlation (exp. ST2) led to a reduction in annual national total $FFCO_2$ of 33 TgC/yr, or 2% relative to the default setup, and a similar spatial pattern of change to experiment ST1. As might be expected, the change in temporal correlation length also produced small changes to the seasonal cycle of $FFCO_2$ at the national scale, but these are primarily small reductions in March through July (Fig. S6) that lie within derived monthly posterior flux uncertainties of 3-6%. Finally, changing the spatial error correlation length of NBE

https://doi.org/10.5194/egusphere-2026-2896
Preprint. Discussion started: 6 July 2026

adjustment (exp. ST3) had no discernible impact on the derived national total and little spatially coherent impact on the $FFCO_2$ distribution (Fig. S5). Given that the impact of all three sensitivity experiments on derived annual national totals is similar to or less than the range of the MC-derived random 1σ posterior uncertainties, this finding suggests that results obtained using the 9-member ensemble employing the default hybrid treatment are determined primarily by the observations and not the specified spatiotemporal covariance parameters determining B.

3.4.4 Constraining fluxes within and between regions

The primary advantage of assimilating $\Delta^{14}C$ and CO_2 observations in a dual tracer inversion system such as the one used here is the ability to simultaneously derive both NBE and $FFCO_2$ flux, in contrast to CO_2-only inversions in which fossil emissions are fixed. From an idealized mass-balance point of view (e.g., (Levin et al., 2003; Turnbull et al., 2006), $\Delta^{14}C$ measurements map directly onto $FFCO_2$, while NBE is determined from the residual difference of total CO_2 flux and $FFCO_2$, where total net CO_2 flux is constrained by CO_2 mole fraction observations. To a good approximation, $FFCO_2$ uncertainty is a function of the frequency and spatial distribution of $\Delta^{14}C$ observations, while NBE uncertainty is determined by the combined $FFCO_2$ and total CO_2 flux uncertainty. Indeed, approximation of the national, annual NBE uncertainty as the quadrature sum of $FFCO_2$ and total CO_2 uncertainty matches the MC-derived NBE posterior uncertainty (Section 2.4) to within ~5% for both 2010 and 2015 (Table S7), suggesting that the mass-balance based error formulation reasonably represents the more complex inverse system. Given that observations of instantaneous total CO_2 gradients constraining the inverse estimates are dominated by NBE, it is not surprising that uncertainty in the national, annual total carbon balance also drives the uncertainty in derived NBE. This is analogous to the case for CO_2-only inversions in which $FFCO_2$ fluxes are assigned zero uncertainty, except that here $FFCO_2$ and its uncertainties are constrained by observations.

A more formal metric describing the ability of the dual-tracer system to independently resolve flux types (i.e., total CO_2, NBE, and $FFCO_2$) within regions or individual fluxes between regions can be obtained from same the 100-member MC ensembles used to estimate random posterior flux uncertainty (Section 2.4) (Table 5). In this case, the off-diagonal elements of $\widehat{B}$ are analyzed to yield the correlations between posterior estimates of any two flux types or regions (Basu et al., 2016; Basu et al., 2020). Using this approach, we find correlation (r) between total CO_2 and NBE of 0.77 in 2010 and 0.65 (i.e., r closer to 1 than 0) in 2015 for the U.S. as a whole, supporting the notion that uncertainty in total CO_2 is contributing significantly to uncertainty in NBE at this scale. For NBE and $FFCO_2$, posterior correlations are only somewhat smaller in magnitude (-0.60 for 2010 and -0.56 for 2015) but of negative sign, indicating that inability to perfectly separate these two sources drives much of the posterior uncertainty in $FFCO_2$ in each region. It is important to note, however, that overall MC-derived uncertainties in national total $FFCO_2$ are relatively small (<2% at 1σ) underscoring a substantial ability of the system to constrain $FFCO_2$ flux. Comparable negative posterior correlations of NBE and $FFCO_2$ also hold true at the regional scale (Table 5). Non-negligible negative error correlations for NBE and $FFCO_2$ suggest that overall $FFCO_2$ flux uncertainty can be further reduced at both national and regional scale by increasing observational coverage of $\Delta^{14}CO_2$. In contrast to findings for total net CO_2 and NBE, the posterior

https://doi.org/10.5194/egusphere-2026-2896
Preprint. Discussion started: 6 July 2026

error correlations between total net CO_2 and $FFCO_2$ at the national scale are generally significantly smaller (0.06 in 2010 and 0.27 in 2015), consistent with the fact that at any one time, national scale CO_2 gradients are dominated by the pattern of NBE (and generally not by $FFCO_2$).

For annual total $FFCO_2$ in individual U.S. regions for both 2010 and 2015 we obtain random posterior uncertainties ranging from 6% to 22% (east < central < west, based on single year values in Table 3), as discussed in Section 3.3. However, posterior flux correlations are generally not larger than 0.1 between any combination of regions (Table 5), indicating that the inversion system resolves $FFCO_2$ independently amongst all three U.S. regions despite relatively high posterior uncertainty in the Central and Western U.S.

We also determined posterior correlations between U.S. annual total $FFCO_2$ and $FFCO_2$ and NBE fluxes in Eurasia, and between U.S. annual total $FFCO_2$ and disequilibrium fluxes within and outside the U.S. (Table 5). U.S. $FFCO_2$ flux estimates in both 2010 and 2015 display negligible correlation (95 % CIs encompassing zero) with uncertainties for $FFCO_2$ and NBE in China and for Eurasian Boreal NBE (the region as defined per Gurney et al. (2002)). However, there remains non-negligible correlation between U.S. $FFCO_2$ and U.S. biospheric disequilibrium fluxes in both years, and between U.S. $FFCO_2$ and upwind North Pacific Ocean disequilibrium fluxes in 2015, suggesting that improved observational constraints over these areas would improve U.S. $FFCO_2$ estimates. In the current system, we intentionally specify relatively large *a priori* uncertainties for disequilibrium fluxes outside the U.S. target domain (Table S2) in order to allow for additional flux adjustment in regions with relatively few ^{14}C observations. This approach provides for improved representation of $\Delta^{14}C$ of air entering the target domain (against which $FFCO_2$ related $\Delta^{14}CO_2$ anomalies are theoretically quantified) but also adds to derived posterior $FFCO_2$ flux uncertainty (as all *a priori* fluxes are randomly perturbed in the determination of MC-derived posterior flux uncertainty, per Section 2.4). Expansion of ^{14}C observations in more remote regions would reduce the need for such generous *a priori* uncertainties. In addition, such observations would improve observational constraints on derived far-field disequilibrium fluxes which are also of interest in carbon cycle studies, since they scale directly to often ill-quantified one-way gross mass fluxes of carbon over land and the oceans (Miller et al., 2025a; Miller et al., 2025b).

https://doi.org/10.5194/egusphere-2026-2896
Preprint. Discussion started: 6 July 2026

Table 5: Correlations of posterior flux uncertainties across the 100 MC simulations for each year using the Miller/CT2022 $FFCO_2$ and CT2016 NBE flux priors. Uncertainties of the posterior correlations are given at their respective 95% CIs, as described in the text. MC simulations are those used to derive analytical posterior uncertainties as discussed in Section 2.4.

correlate fluxes	correlate regions/quantities		2010	2015
	correlate A	correlate B	posterior correlation [95% CI]	posterior correlation [95% CI]
FF vs. FF for U.S. regions	Eastern U.S.	Central U.S.	-0.06 [-0.25, 0.13]	0.04 [-0.12, 0.21]
	Eastern U.S.	Western U.S.	-0.11 [-0.31, 0.10]	0.15 [-0.03, 0.33]
	Eastern U.S.	Central + Western U.S.	-0.11 [-0.31, 0.09]	0.12 [-0.03, 0.26]
	Central U.S.	Western U.S.	0.11 [-0.10, -0.31]	-0.02 [-0.24, 0.19]
	Central U.S.	Eastern + Western U.S.	0 [-0.19, 0.19]	0.03 [-0.16, 0.21]
	Western U.S.	Eastern + Central U.S.	-0.03 [-0.19, 0.15]	0.1 [-0.11, 0.31]
FF vs. NBE for US and US regions	U.S. FF	U.S. NBE	-0.60 [-0.72, -0.46]	-0.56 [-0.66, -0.43]
	Eastern U.S. FF	Eastern U.S. NBE	-052. [-0.65, -0.35]	-0.60 [-0.7, -0.46]
	Western U.S. FF	Western U.S. NBE	-0.45 [-0.61, -0.26]	-0.34 [-0.52, -0.13]
	Central U.S. FF	Central U.S. NBE	-0.5 [-0.64, -0.34]	-0.62 [-0.74, -0.46]
US FF vs. FF or NBE in remote regions	U.S. FF	China FF	0 [-0.18, 0.19]	-0.10 [-0.28, 0.08]
	U.S. FF	China NBE	0.06 [-0.15, 0.26]	-0.03 [-0.24, 0.17]
	U.S. FF	Eurasia Boreal NBE	0.10 [-0.11, 0.30]	0.04 [-0.13, 0.21]
FF vs. disequilibrium	U.S. FF	U.S. bio disequ.	0.31 [0.13, 0.47]	0.55 [0.41, 0.66]
	U.S. FF	N. Pacific Ocean disequ.	0.29 [0.10, 0.46]	0.02 [-0.18, 0.22]
FF or NBE vs. Total Carbon	U.S. FF	U.S. Total Carbon	0.06 [-0.16, 0.26]	0.27 [0.11, 0.42]
	U.S. NBE	U.S. Total Carbon	0.77 [0.68, 0.84]	0.65 [0.52, 0.75]

https://doi.org/10.5194/egusphere-2026-2896
Preprint. Discussion started: 6 July 2026

4 Conclusions

Here we provide new U.S. national and regional annual and monthly $FFCO_2$ estimates for the years 2010 and 2015 obtained from the dual-tracer (^{14}C and CO_2) inversion system of Basu et al. (2016) and Basu et al. (2020). System updates to the inversion framework include increases to prior flux uncertainties, use of an updated CO_2 ObsPack (GLOBALVIEW+6.1, (Schuldt et al., 2021), updated atmospheric transport (ERA5, Hersbach et al. (2020)), and changes to the Miller/CarbonTracker prior $FFCO_2$ distribution used as the default $FFCO_2$ prior in our previous work. The total impact of these changes on derived national $FFCO_2$ totals was +118 TgC/yr relative to the estimate of 1627 ± 30 TgC/yr (1σ) obtained previously for 2010 using the original experimental set up of Basu et al. (2020). By far the largest impacts on the difference in derived total was from the change in spatial pattern of $FFCO_2$ emission in the updated Miller/CarbonTracker $FFCO_2$ prior and the increase in the number of CO_2 observations in the updated CO_2 ObsPack. Other impacts were smaller than the updated analytical posterior $FFCO_2$ uncertainty of 1.6% (1σ).

In order to provide a more complete characterization of posterior $FFCO_2$ uncertainties, for each year we ran an expanded ensemble of 9 experiments using a combination of 3 different $FFCO_2$ priors (including the Miller/CarbonTracker update) and 3 different NBE priors, allowing us to compare formally-derived random posterior uncertainties for individual experiments with ensemble-wide spread and standard deviation. For 2010, the observed uncertainty-weighted ensemble-wide mean U.S. national total $FFCO_2$ is 1715 TgC/yr with an ensemble-wide 2σ spread of 88 TgC/yr and 1σ posterior uncertainties for individual ensemble members ranging from 26 to 49 TgC/yr. For 2015 the observed national total is 1578 TgC/yr with a 2σ ensemble-wide spread of 116 TgC/yr and single-member 1σ experimental posterior uncertainties ranging from 29 to 37 TgC/yr. In both years, the ensembles display statistically robust deviations from prior $FFCO_2$ for all months (with the single exception of April 2015), with annual national totals that agree with adjusted national totals from the Vulcan 3.0 data product to within 1σ, ensemble wide. Sixteen of 24 derived monthly totals and 12 of 15 tri-monthly seasonal totals also agree with adjusted monthly or tri-monthly Vulcan totals to within 1σ, ensemble wide.

Changes in derived ensemble mean $FFCO_2$ between 2010 and 2015 indicate a reduction in emissions of 7.8 ±3.0% (2σ, ensemble wide) over the interval, compared to 5.8% and 5.1% for central estimates from Vulcan and EPA, respectively. The change in $FFCO_2$ indicated by the atmospheric observations is statistically robust and broadly consistent with the central estimates from Vulcan and EPA which together indicate a decrease of U.S. emission of at least 5% from 2010 and 2015. An analysis of regional emissions results indicates that the bulk of the emissions reduction occurred in the Eastern U.S., in agreement with expectations based on the transition to lower carbon fuels in the disproportionately large, regional power sector.

https://doi.org/10.5194/egusphere-2026-2896
Preprint. Discussion started: 6 July 2026

We evaluate the robustness of our findings in several ways, including the ability of the system to represent the assimilated CO_2 and ^{14}C observations both before and after flux optimization, relative system sensitivity to specified $FFCO_2$ and NBE priors, sensitivity to choice of spatial and temporal correlation characteristics of prior flux uncertainties, and the ability of the system to independently resolve $FFCO_2$ fluxes between different U.S. census regions (Eastern, Central and Western) and different flux types (total CO_2, $FFCO_2$, NBE) for the U.S. as a whole and within regions. The overall finding is that the flux optimization and transport are robust, the system and results remain stable to various (even possible outlier) specifications of fossil and NBE priors, and that the system independently resolves $FFCO_2$ fluxes even for U.S. regions with relatively large posterior flux uncertainties. An analysis of correlations of posterior flux estimates obtained from a large ensemble of perturbation experiments indicates that overall $FFCO_2$ posterior flux uncertainty can be improved at both national and regional scale by additional observational ^{14}C coverage and is not inherently limited by other aspects of the system.

Finally, the strong agreement between the "top down" results from atmospheric observation and those coming, in particular, from the Vulcan project (Gurney et al., 2020a; Gurney et al., 2020b) suggests that the two can be used jointly to provide a scientifically rigorous $FFCO_2$ emissions observing program in which the dual-tracer system described here provides integral constraints on national and regional $FFCO_2$ emission while the "^{14}C-verified" Vulcan results provide information on emissions from individual economic sectors and at smaller spatial scale. This may become especially relevant given the current precarity of previously mandated EPA emissions monitoring efforts.

Code and data availability

The TM5 4DVar inversion framework used in this study is open source and publicly accessible from the sourceforge repository (https://sourceforge.net/projects/tm5/). As indicated in section 2.2 of the main text, our inversion system assimilated CO_2 observations from NOAA's ObsPack GV+6.1 (Schuldt et al., 2021) and $\Delta^{14}CO_2$ observations coming largely from the North American portion of the NOAA Global Greenhouse Gas Reference Network (GGGRN, https://gml.noaa.gov/ccgg/about.html) (Andrews et al., 2014; Sweeney et al., 2015). Additional observations were obtained from the $\Delta^{14}C$ measurement programs at the University of Heidelberg (Levin et al., 2023), the University of California, Irvine, and Rafter Radiocarbon Laboratory, Earth Sciences New Zealand (Table S1).

Author contributions

SMNI, SJL and JBM wrote the paper; SJL, JBM and SB guided the analysis; SMNI performed the experiments with assistance from SB.

https://doi.org/10.5194/egusphere-2026-2896
Preprint. Discussion started: 6 July 2026

Competing interests

The authors declare that they have no conflicts of interest.

Acknowledgements

CO_2 measurements were courtesy of the data providers to ObsPack GLOBALVIEW+ 6.1, including ICOS and its contributing investigators (https://www.icos-cp.eu). Univ. of Heidelberg ^{14}C measurements were provided by Dr. Samuel Hammer and INX ^{14}C measurements were provided by Dr. Jocelyn Turnbull, Rafter Radiocarbon Laboratory, Earth Sciences New Zealand. Dr. Andrew Jacobson kindly reviewed the manuscript.

Financial support

This work was funded by NOAA AC4 award NA19OAR4310166 to SJL and JBM with additional support from NOAA GML. SB acknowledges funding from NASA through cooperative agreement 80NSSC23M0011 with the University of Maryland.

References

Andrews, A. E., Kofler, J. D., Trudeau, M. E., Williams, J. C., Neff, D. H., Masarie, K. A., Chao, D. Y., Kitzis, D. R., Novelli, P. C., Zhao, C. L., Dlugokencky, E. J., Lang, P. M., Crotwell, M. J., Fischer, M. L., Parker, M. J., Lee, J. T., Baumann, D. D., Desai, A. R., Stanier, C. O., De Wekker, S. F. J., Wolfe, D. E., Munger, J. W., and Tans, P. P.: CO_2, CO, and CH_4 measurements from tall towers in the NOAA Earth System Research Laboratory's Global Greenhouse Gas Reference Network: instrumentation, uncertainty analysis, and recommendations for future high-accuracy greenhouse gas monitoring efforts, Atmos. Meas. Tech., 7, 647-687, 10.5194/amt-7-647-2014, 2014.

Asefi-Najafabady, S., Rayner, P. J., Gurney, K. R., McRobert, A., Song, Y., Coltin, K., Huang, J., Elvidge, C., and Baugh, K.: A multiyear, global gridded fossil fuel CO_2 emission data product: Evaluation and analysis of results, Journal of Geophysical Research: Atmospheres, 119, 10,213-210,231, 10.1002/2013JD021296, 2014.

Basu, S., Miller, J. B., and Lehman, S.: Separation of biospheric and fossil fuel fluxes of CO_2 by atmospheric inversion of CO_2 and $^{14}CO_2$ measurements: Observation System Simulations, Atmos. Chem. Phys., 16, 5665-5683, 10.5194/acp-16-5665-2016, 2016.

Basu, S., Lehman, S. J., Miller, J. B., Andrews, A. E., Sweeney, C., Gurney, K. R., Xu, X., Southon, J., and Tans, P. P.: Estimating US fossil fuel CO_2 emissions from measurements of ^{14}C in atmospheric CO_2, Proceedings of the National Academy of Sciences, 117, 13300-13307, 10.1073/pnas.1919032117, 2020.

Byrne, B., Baker, F. D., Basu, S., Bertolacci, M., Bowman, W. K., Carroll, D., Chatterjee, A., Chevallier, F., Ciais, P., Cressie, N., Crisp, D., Crowell, S., Deng, F., Deng, Z., Deutscher, M. N., Dubey, K. M., Feng, S., García, E. O., Griffith, T. W. D., Herkommer, B., Hu, L., Jacobson, R. A., Janardanan, R., Jeong, S., Johnson, S. M., Jones, A. B. D., Kivi, R., Liu, J., Liu, Z., Maksyutov, S., Miller, B. J., Miller, M. S., Morino, I., Notholt, J., Oda, T., O'Dell, W. C., Oh, Y.-S., Ohyama, H., Patra, K. P., Peiro, H., Petri, C., Philip, S., Pollard, F. D., Poulter, B., Remaud, M., Schuh, A., Sha, K. M., Shiomi, K., Strong, K., Sweeney, C., Té, Y., Tian, H., Velazco, A. V., Vrekoussis, M., Warneke, T., Worden, R. J., Wunch, D., Yao, Y., Yun, J., Zammit-Mangion, A., and Zeng, N.: National CO_2 budgets (2015–2020) inferred from atmospheric CO_2 observations in support of the global stocktake, Earth System Science Data, 15, 963-1004, https://doi.org/10.5194/essd-15-963-2023, 2023.

https://doi.org/10.5194/egusphere-2026-2896
Preprint. Discussion started: 6 July 2026

Crippa, M., Oreggioni, G., Guizzardi, D., Muntean, M., Schaaf, E., Lo Vullo, E., Solazzo, E., Monforti-Ferrario, F., Olivier, J., and Vignati, E.: Fossil CO2 and GHG emissions of all world countries, Luxembourg (Luxembourg), 10.2760/687800 (online),10.2760/655913 (print), 2019.

Crippa, M., Guizzardi, D., Pagani, F., Banja, M., Muntean, M., Schaaf, E., Monforti-Ferrario, F., Becker, W.E., Quadrelli, R., Risquez Martin, A., Taghavi-Moharamli, P., Köykkä, J., Grassi, G., Rossi, S., Melo, J., Oom, D., Branco, A., San-Miguel, J., Manca, G., Pisoni, E., Vignati, E. and Pekar, F.: GHG emissions of all world countries, Publications Office of the European Union, Luxembourg, doi:10.2760/4002897, 2024.

EIA: Monthly Energy Review: Population-weighted degree days, https://www.eia.gov/energyexplained/units-and-calculators/degree-days.php, 2024.

EPA: Inventory of U.S. Greenhouse Gas Emissions and Sinks: 1990-2022 U.S. Environmental Protection Agency, EPA 430R-24004, https://www.epa.gov/ghgemissions/inventory-us-greenhouse-gas-emissions-and-sinks-1990-2022, 2024a.

EPA: State GHG Emissions and Removals, https://www.epa.gov/ghgemissions/state-ghg-emissions-and-removals, 2024b.

Graven, H. D., Guilderson, T. P., and Keeling, R. F.: Observations of radiocarbon in CO2 at seven global sampling sites in the Scripps flask network: Analysis of spatial gradients and seasonal cycles, Journal of Geophysical Research: Atmospheres, 117, 10.1029/2011jd016535, 2012.

Gurney, K. R., Liang, J., Patarasuk, R., Song, Y., Huang, J., and Roest, G.: Vulcan: High-Resolution Annual Fossil Fuel CO2 Emissions in USA, 2010-2015, Version 3, ORNL Distributed Active Archive Center [dataset], 10.3334/ORNLDAAC/1810, 2020a.

Gurney, K. R., Liang, J., Patarasuk, R., Song, Y., Huang, J., and Roest, G.: The Vulcan Version 3.0 High-Resolution Fossil Fuel CO2 Emissions for the United States, Journal of Geophysical Research: Atmospheres, 125, e2020JD032974, https://doi.org/10.1029/2020JD032974, 2020b.

Gurney, R. K., Law, M. R., Denning, S. A., Rayner, J. P., Baker, D., Bousquet, P., Bruhwiler, L., Chen, Y.-H., Ciais, P., Fan, S., Fung, Y. I., Gloor, M., Heimann, M., Higuchi, K., John, J., Maki, T., Maksyutov, S., Masarie, K., Peylin, P., Prather, M., Pak, C. B., Randerson, J., Sarmiento, J., Taguchi, S., Takahashi, T., and Yuen, C.-W.: Towards robust regional estimates of CO_2 sources and sinks using atmospheric transport models, Nature, 415, 626-630, https://doi.org/10.1038/415626a, 2002.

Haynes, K., Baker, I., and Denning, S.: The Simple Biosphere Model Version 4.2: SiB4 Technical Description, 2020.

Hersbach, H., Bell, B., Berrisford, P., Hirahara, S., Horányi, A., Muñoz-Sabater, J., Nicolas, J., Peubey, C., Radu, R., Schepers, D., Simmons, A., Soci, C., Abdalla, S., Abellan, X., Balsamo, G., Bechtold, P., Biavati, G., Bidlot, J., Bonavita, M., Chiara, D. G., Dahlgren, P., Dee, D., Diamantakis, M., Dragani, R., Flemming, J., Forbes, R., Fuentes, M., Geer, A., Haimberger, L., Healy, S., Hogan, J. R., Hólm, E., Janisková, M., Keeley, S., Laloyaux, P., Lopez, P., Lupu, C., Radnoti, G., Rosnay, D. P., Rozum, I., Vamborg, F., Villaume, S., and Thépaut, J. N.: The ERA5 global reanalysis, Quarterly Journal of the Royal Meteorological Society, 146, 1999-2049, https://doi.org/10.1002/qj.3803, 2020.

IPCC, [Masson-Delmotte, V., P. Zhai, H.-O. Pörtner, D. Roberts, J. Skea, P.R. Shukla, A. Pirani, W. Moufouma-Okia, C. Péan, R. Pidcock, S. Connors, J.B.R. Matthews, Y. Chen, X. Zhou, M.I. Gomis, E. Lonnoy, T. Maycock, M. Tignor, and T. Waterfield (eds.) (Ed.): Global Warming of 1.5°C. An IPCC Special Report on the impacts of global warming of 1.5°C above pre-industrial levels and related global greenhouse gas emission pathways, in the context of strengthening the global response to the threat of climate change, sustainable development, and efforts to eradicate poverty, Cambridge University Press, Cambridge, UK and New York, NY, USA, 616 pp., https://doi.org/10.1017/9781009157940., 2018.

Jacobson, A. R., Schuldt, K. N., Miller, J. B., Oda, T., Tans, P., Arlyn, A., Mund, J., Ott, L., Collatz, G. J., Aalto, T., Afshar, S., Aikin, K., Aoki, S., Apadula, F., Baier, B., Bergamaschi, P., Beyersdorf, A., Biraud, S. C., Bollenbacher, A., Bowling, D., Brailsford, G., Abshire, J. B., Chen, G., Huilin, C., Lukasz, C., Sites, C., Colomb, A., Conil, S., Cox, A., Cristofanelli, P., Cuevas, E., Curcoll, R., Sloop, C. D., Davis, K., Wekker, S. D., Delmotte, M., DiGangi, J. P., Dlugokencky, E., Ehleringer, J., Elkins, J. W., Emmenegger, L., Fischer, M. L., Forster, G., Frumau, A., Galkowski, M., Gatti, L. V., Gloor, E., Griffis, T., Hammer, S., Haszpra, L., Hatakka, J., Heliasz, M., Hensen, A., Hermanssen, O., Hintsa, E., Holst, J., Jaffe, D., Karion, A., Kawa, S. R., Keeling, R., Keronen, P., Kolari, P., Kominkova, K., Kort, E., Krummel, P., Kubistin, D., Labuschagne, C., Langenfelds, R., Laurent, O., Laurila, T., Lauvaux, T., Law, B., Lee, J., Lehner, I., Leuenberger, M., Levin, I., Levula, J., Lin, J., Lindauer, M., Loh, Z., Lopez, M., Luijkx, I. T., Myhre, C. L., Machida, T., Mammarella, I., Manca, G., Manning, A., Manning, A., Marek, M. V., Marklund, P., Martin, M. Y., Matsueda, H., McKain, K., Meijer, H., Meinhardt, F., Miles, N., Miller, C. E., Mölder, M., Montzka, S., Moore, F., Josep-Anton, M., Morimoto, S., Munger, B., Jaroslaw, N., Newman, S., Nichol, S., Niwa, Y., O'Doherty, S., Mikaell, O.-L., Paplawsky, B., Peischl, J., Peltola, O., Jean-Marc, P., Piper, S., Plass-

https://doi.org/10.5194/egusphere-2026-2896
Preprint. Discussion started: 6 July 2026

Dölmer, C., Ramonet, M., Reyes-Sanchez, E., Richardson, S., Riris, H., Ryerson, T., Saito, K., Sargent, M., Sasakawa, M., Sawa, Y., Say, D., Scheeren, B., Schmidt, M., Schmidt, A., Schumacher, M., Shepson, P., Shook, M., Stanley, K., Steinbacher, M., Stephens, B., Sweeney, C., Thoning, K., Torn, M., Turnbull, J., Tørseth, K., Bulk, P. V. D., Dinther, D. V., Vermeulen, A., Viner, B., Vitkova, G., Walker, S., Weyrauch, D., Wofsy, S., Worthy, D., Dickon, Y., and Miroslaw, Z.: CarbonTracker CT2019B, 10.25925/20201008, 2020.

Jacobson, A. R., Schuldt, K. N., Tans, P., Arlyn, A., Miller, J. B., Oda, T., Mund, J., Weir, B., Ott, L., Aalto, T., Abshire, J. B., Aikin, K., Aoki, S., Apadula, F., Arnold, S., Baier, B., Bartyzel, J., Beyersdorf, A., Biermann, T., Biraud, S. C., Boenisch, H., Brailsford, G., Brand, W. A., Chen, G., Huilin, C., Lukasz, C., Clark, S., Colomb, A., Commane, R., Conil, S., Couret, C., Cox, A., Cristofanelli, P., Cuevas, E., Curcoll, R., Daube, B., Davis, K. J., De Wekker, S., Coletta, J. D., Delmotte, M., DiGangi, E., DiGangi, J. P., Di Sarra, A. G., Dlugokencky, E., Elkins, J. W., Emmenegger, L., Shuangxi, F., Fischer, M. L., Forster, G., Frumau, A., Galkowski, M., Gatti, L. V., Gehrlein, T., Gerbig, C., Francois, G., Gloor, E., Gomez-Trueba, V., Goto, D., Griffis, T., Hammer, S., Hanson, C., Haszpra, L., Hatakka, J., Heimann, M., Heliasz, M., Hensen, A., Hermansen, O., Hintsa, E., Holst, J., Ivakhov, V., Jaffe, D. A., Jordan, A., Joubert, W., Karion, A., Kawa, S. R., Kazan, V., Keeling, R. F., Keronen, P., Kneuer, T., Kolari, P., Kateřina, K., Kort, E., Kozlova, E., Krummel, P., Kubistin, D., Labuschagne, C., Lam, D. H. Y., Lan, X., Langenfelds, R. L., Laurent, O., Laurila, T., Lauvaux, T., Lavric, J., Law, B. E., Lee, J., Lee, O. S. M., Lehner, I., Lehtinen, K., Leppert, R., Leskinen, A., Leuenberger, M., Levin, I., Levula, J., Lin, J., Lindauer, M., Loh, Z., Lopez, M., Luijkx, I. T., Lunder, C. R., Machida, T., Mammarella, I., Manca, G., Manning, A., Manning, A., Marek, M. V., Martin, M. Y., Matsueda, H., McKain, K., Meijer, H., Meinhardt, F., Merchant, L., Mihalopoulos, N., Miles, N. L., Miller, C. E., Mitchell, L., Mölder, M., Montzka, S., Moore, F., Moossen, H., Morgan, E., Josep-Anton, M., Morimoto, S., Müller-Williams, J., Munger, J. W., Munro, D., Myhre, C. L., Shin-Ichiro, N., Jaroslaw, N., Newman, S., Nichol, S., Niwa, Y., Obersteiner, F., O'Doherty, S., Paplawsky, B., Peischl, J., Peltola, O., Piacentino, S., Jean-Marc, P., Pickers, P., Piper, S., Pitt, J., Plass-Dülmer, C., Platt, S. M., Prinzivalli, S., Ramonet, M., Ramos, R., Reyes-Sanchez, E., Richardson, S. J., Riris, H., Rivas, P. P., Ryerson, T., Saito, K., Sargent, M., Sasakawa, M., Scheeren, B., Schuck, T., Schumacher, M., Seifert, T., Sha, M. K., Shepson, P., Shook, M., Sloop, C. D., Smith, P., Stanley, K., Steinbacher, M., Stephens, B., Sweeney, C., Thoning, K., Timas, H., Torn, M., Tørseth, K., Trisolino, P., Turnbull, J., Van Den Bulk, P., Van Dinther, D., Vermeulen, A., Viner, B., Vitkova, G., Walker, S., Watson, A., Wofsy, S. C., Worsey, J., Worthy, D., Dickon, Y., Zaehle, S., Zahn, A., and Miroslaw, Z.: CarbonTracker CT2022, 10.25925/Z1GJ-3254, 2023.

Kato, A., Gurney, K. R., Roest, G. S., and Dass, P.: Exploring differences in FFCO2 emissions in the United States: comparison of the Vulcan data product and the EPA national GHG inventory, Environmental Research Letters, 18, 10.1088/1748-9326/ad0b22, 2023.

Lehman, S. J., Miller, J. B., Wolak, C., Southon, J., Tans, P. P., Montzka, S. A., Sweeney, C., Andrews, A., LaFranchi, B., Guilderson, T. P., and Turnbull, J. C.: Allocation of Terrestrial Carbon Sources Using 14CO2: Methods, Measurement, and Modeling, Radiocarbon, 55, 1484-1495, 10.1017/S0033822200048414, 2013.

Levin, I., Kromer, B., Schmidt, M., and Sartorius, H.: A novel approach for independent budgeting of fossil fuel CO_2 over Europe by $^{14}CO_2$ observations, Geophysical Research Letters, 30, doi:10.1029/2003GL018477, 2003.

Levin, I., Preunkert, S., Graven, H., Lewis, C., Miller, J. B., Turnbull, J. C., Xu, X., and Hammer, S.: CO2MVS RESEARCH ON SUPPLEMENTARY OBSERVATIONS: Database of existing Delta$^{14}CO_2$ measurements, 2023.

Liu, Z., Deng, Z., Davis, J. S., and Ciais, P.: Global carbon emissions in 2023, Nature Reviews Earth & Environment, 5, 253-254, https://doi.org/10.1038/s43017-024-00532-2, 2024.

Liu, Z., Ciais, P., Deng, Z., Davis, J. S., Zheng, B., Wang, Y., Cui, D., Zhu, B., Dou, X., Ke, P., Sun, T., Guo, R., Zhong, H., Boucher, O., Bréon, F.-M., Lu, C., Guo, R., Xue, J., Boucher, E., Tanaka, K., and Chevallier, F.: Carbon Monitor, a near-real-time daily dataset of global CO_2 emission from fossil fuel and cement production, Scientific Data, 7, https://doi.org/10.1038/s41597-020-00708-7, 2020.

Miller, B. J., Lehman, J. S., Montzka, A. S., Sweeney, C., Miller, R. B., Karion, A., Wolak, C., Dlugokencky, J. E., Southon, J., Turnbull, C. J., and Tans, P. P.: Linking emissions of fossil fuel CO_2 and other anthropogenic trace gases using atmospheric $^{14}CO_2$, Journal of Geophysical Research: Atmospheres, 117, https://doi.org/10.1029/2011JD017048, 2012.

Miller, J. B., Lehman, S. J., and Lindsay, C. M.: Numerical Representation of Contemporary Atmospheric Δ14CO2: 1. Time-Varying Global Fluxes and Atmospheric Mass Balance, Global Biogeochemical Cycles, 39, e2025GB008522, https://doi.org/10.1029/2025GB008522, 2025a.

https://doi.org/10.5194/egusphere-2026-2896
Preprint. Discussion started: 6 July 2026

Miller, J. B., Lehman, S. J., Andrews, A., Sweeney, C., McKain, K., Tans, P., Southon, J., Hammer, S., Turnbull, J., and Xu, X.: Numerical Representation of Contemporary Atmospheric Δ14CO2: 2. Three-Dimensional Simulation and Comparison With Observations, Global Biogeochemical Cycles, 39, 10.1029/2025gb008523, 2025b.

Oda, T. and Maksyutov, S.: ODIAC Fossil Fuel CO2 Emissions Dataset (ODIAC2022) [dataset], doi:10.17595/20170411.001, 2015.

Oda, T., Maksyutov, S., and Andres, R. J.: The Open-source Data Inventory for Anthropogenic CO_2, version 2016 (ODIAC2016): a global monthly fossil fuel CO_2 gridded emissions data product for tracer transport simulations and surface flux inversions, Earth System Science Data, 10, 87-107, 10.5194/essd-10-87-2018, 2018.

Peters, W., Jacobson, R. A., Sweeney, C., Andrews, E. A., Conway, J. T., Masarie, K., Miller, B. J., Bruhwiler, P. M. L., Pétron, G., Hirsch, I. A., Worthy, J. E. D., Werf, D. V. R. G., Randerson, T. J., Wennberg, O. P., Krol, C. M., and Tans, P. P.: An atmospheric perspective on North American carbon dioxide exchange: CarbonTracker, Proceedings of the National Academy of Sciences, 104, 18925-18930, https://doi.org/10.1073/pnas.0708986104, 2007.

Potier, E., Broquet, G., Wang, Y., Santaren, D., Berchet, A., Pison, I., Marshall, J., Ciais, P., Bréon, F.-M., and Chevallier, F.: Complementing XCO_2 imagery with ground-based CO_2 and $^{14}CO_2$ measurements to monitor CO_2 emissions from fossil fuels on a regional to local scale, Atmospheric Measurement Techniques, 15, 5261-5288, 10.5194/amt-15-5261-2022, 2022.

Schuldt, K. N., Mund, J., Luijkx, I. T., Aalto, T., Abshire, J. B., Aikin, K., Arlyn, A., Aoki, S., Apadula, F., Baier, B., Bakwin, P., Bartyzel, J., Bentz, G., Bergamaschi, P., Beyersdorf, A., Biermann, T., Biraud, S. C., Boenisch, H., Bowling, D., Brailsford, G., Van Den Bulk, P., Chen, G., Huilin, C., Lukasz, C., Clark, S., Sites, C., Coletta, J. D., Colomb, A., Commane, R., Conil, S., Cox, A., Cristofanelli, P., Cuevas, E., Curcoll, R., Daube, B., Davis, K., Delmotte, M., DiGangi, J. P., Van Dinther, D., Dlugokencky, E., Elkins, J. W., Emmenegger, L., Shuangxi, F., Fischer, M. L., Forster, G., Frumau, A., Galkowski, M., Gatti, L. V., Gehrlein, T., Gerbig, C., Francois, G., Gloor, E., Gomez-Trueba, V., Goto, D., Griffis, T., Hammer, S., Hanson, C., Haszpra, L., Hatakka, J., Heimann, M., Heliasz, M., Hensen, A., Hermanssen, O., Hintsa, E., Holst, J., Jaffe, D., Joubert, W., Karion, A., Kawa, S. R., Kazan, V., Keeling, R., Keronen, P., Kolari, P., Kominkova, K., Kort, E., Kozlova, E., Krummel, P., Kubistin, D., Labuschagne, C., Lam, D. H. Y., Langenfelds, R., Laurent, O., Laurila, T., Lauvaux, T., Law, B., Lee, J., Lee, O. S. M., Lehner, I., Leppert, R., Leuenberger, M., Levin, I., Levula, J., Lin, J., Lindauer, M., Loh, Z., Lopez, M., Machida, T., Mammarella, I., Manca, G., Manning, A., Manning, A., Marek, M. V., Martin, M. Y., Matsueda, H., De Mazière, M., McKain, K., Meijer, H., Meinhardt, F., Merchant, L., Mihalopoulos, N., Miles, N., Miller, C. E., Miller, J. B., Mitchell, L., Mölder, M., Montzka, S., Moore, F., Morgan, E., Josep-Anton, M., Morimoto, S., Müller-Williams, J., Munger, B., Myhre, C. L., Jaroslaw, N., Newman, S., Nichol, S., Niwa, Y., O'Doherty, S., Obersteiner, F., Paplawsky, B., Peischl, J., Peltola, O., Pichon, J. M., Piper, S., Plass-Duelmer, C., Plass-Duelmer, C., Ramonet, M., Ramos, R., Reyes-Sanchez, E., Richardson, S., Riris, H., Rivas, P. P., Ryerson, T., Saito, K., Sargent, M., Sasakawa, M., Sawa, Y., Say, D., Scheeren, B., Schuck, T., Schumacher, M., Seifert, T., Sha, M. K., Shepson, P., Shook, M., Sloop, C. D., Smith, P., Steinbacher, M., Stephens, B., Sweeney, C., Tans, P., Thoning, K., Timas, H., Torn, M., Tørseth, K., Trisolino, P., Turnbull, J., Vermeulen, A., Viner, B., Vitkova, G., Walker, S., Watson, A., De Wekker, S., Wofsy, S., Worsey, J., Worthy, D., Dickon, Y., Zahn, A., and Miroslaw, Z.: Multi-laboratory compilation of atmospheric carbon dioxide data for the period 1957-2019; obspack_co2_1_GLOBALVIEWplus_v6.1_2021-03-01, NOAA Global Monitoring Laboratory [dataset], 10.25925/20201204, 2021.

Sitch, S., Friedlingstein, P., Gruber, N., Jones, S. D., Murray-Tortarolo, G., Ahlström, A., Doney, S. C., Graven, H., Heinze, C., Huntingford, C., Levis, S., Levy, P. E., Lomas, M., Poulter, B., Viovy, N., Zaehle, S., Zeng, N., Arneth, A., Bonan, G., Bopp, L., Canadell, J. G., Chevallier, F., Ciais, P., Ellis, R., Gloor, M., Peylin, P., Piao, S. L., Le Quéré, C., Smith, B., Zhu, Z., and Myneni, R.: Recent trends and drivers of regional sources and sinks of carbon dioxide, Biogeosciences, 12, 653-679, 10.5194/bg-12-653-2015, 2015.

Sweeney, C., Karion, A., Wolter, S., Newberger, T., Guenther, D., Higgs, J. A., Andrews, A. E., Lang, P. M., Neff, D., Dlugokencky, E., Miller, J. B., Montzka, S. A., Miller, B. R., Masarie, K. A., Biraud, S. C., Novelli, P. C., Crotwell, M., Crotwell, A. M., Thoning, K., and Tans, P. P.: Seasonal climatology of CO2 across North America from aircraft measurements in the NOAA/ESRL Global Greenhouse Gas Reference Network, Journal of Geophysical Research: Atmospheres, 120, 5155-5190, https://doi.org/10.1002/2014JD022591, 2015.

Turnbull, C. J., Miller, B. J., Lehman, J. S., Tans, P. P., Sparks, J. R., and Southon, J.: Comparison of $^{14}CO_2$, CO, and SF_6 as tracers for recently added fossil fuel CO_2 in the atmosphere and implications for biological CO_2 exchange, Geophysical Research Letters, 33, n/a-n/a, https://doi.org/10.1029/2005GL024213, 2006.

https://doi.org/10.5194/egusphere-2026-2896
Preprint. Discussion started: 6 July 2026

UNFCCC: Adoption of the Paris Agreement, Paris, France, Conference Report, 2015.
Voosen, P.: Al Gore's climate watchdog spots emission gaps, Science, 382, 1096-1097, https://doi.org/10.1126/science.adn3524, 2023.
Wang, Y., Broquet, G., Ciais, P., Chevallier, F., Vogel, F., Kadygrov, N., Wu, L., Yin, Y., Wang, R., and Tao, S.: Estimation of observation errors for large-scale atmospheric inversion of CO_2 emissions from fossil fuel combustion, Tellus B: Chemical and Physical Meteorology, 69, 1325723, https://doi.org/10.1080/16000889.2017.1325723, 2017.